Deep learning reveals the role of copy number variation in the genetic architecture of a highly polymorphic sexual trait

Wouter van der Bijl[1*], Jacelyn J. Shu[1], Versara S. Goberdhan[1], Linley M. Sherin[1], María Cortázar-Chinarro[1,2], Alberto Corral-López[1,2] & Judith E. Mank[1]

1. Department of Zoology & Biodiversity Research Centre, University of British Columbia, Vancouver, Canada

2. Division of Ecology and Genetics, Uppsala University, Uppsala, Sweden

* Corresponding author

Abstract

The extraordinary variation in male guppy coloration has proven a powerful model for studying the interplay of natural and sexual selection. Many guppy populations exhibit substantial Y-linkage of color traits, and this has hampered the identification of the genetic architecture underlying male guppy color, as well as clouded our understanding of how this exceptional level of diversity is maintained. Here we identify the heritability and genetic basis of male color variation using convolutional neural networks for high-resolution phenotyping coupled with selection experiments, controlled pedigrees and whole-genome resequencing for a Genome Wide Association Study (GWAS) of color. Our phenotypic and genomic results converge to show that color patterning in guppies is a combination of many heritable features, each with a partially overlapping genetic architecture spanning the entire genome. Unusually, our GWAS results suggest that copy number variation, particularly copies shared between the Y chromosome and the remainder of the genome, is responsible for much of the variation in color in guppies, providing a potential mechanism for the maintenance of variation of this classic model trait.

24

Introduction

Male guppies, *Poecilia reticulata*, exhibit remarkable variation in coloration, which has been extensively studied in the context of fitness (*1*) and female preference (*2*, *3*). The widespread variation in the extent and patterning of male color across wild populations (*4*, *5*) and the rapid response to natural and artificial selection (*6*, *7*), coupled with high heritability estimates (*8*, *9*) all suggest that substantial genetic variation for this trait is maintained in guppy populations. Although female mate preference for rare male patterns likely acts to preserve some variation from the eroding forces of genetic drift and selection (*2*, *10*, *11*), the genetic architecture underlying extraordinary diversity in male guppy color remains mysterious, as does the maintenance of this exceptional diversity.

Part of the difficulty in determining the genetic basis of male guppy coloration lies in the multiple forms of variation. Yellow-orange xanthophores and black melanophores form spots that vary among males in their location, as well as in the extent and saturation of these colors. Color pattern variation arises from embryonic neural crest cells that form the precursors of xanthophores and melanophores (*12*). Therefore, the genetic basis of color variation is expected to include loci involved in the migration of neural crest cells, as well as genes involved in the synthesis and deposition of pigments. Importantly, orange carotenoids are not synthesized *de novo* in vertebrates, but are collected from food sources (*13*) and modified prior to deposition.

The identification of loci underlying guppy color variation is further complicated by both its genetic architecture, and the complexity of the phenotype. Patterns are largely Y-linked in many populations and faithfully passed on from father to son (*8*, *14–16*), hindering our ability to separate genetic contributions to different pattern elements as they are genetically linked and co-inherited. The color patterns themselves are a combination of spots and lines with varying hues, shapes, and locations, hampering quantification using traditional methods. Here we overcome these longstanding obstacles by

taking advantage of a population with relatively low levels of Y-linkage for color variation (*9*) to identify its heritability and genetic basis. We developed a pipeline of convolutional neural networks for high-resolution phenotyping of 3,229 fish coupled with selection experiments and controlled pedigrees to determine the heritability of specific color elements. Additionally, we introduce a deep learning approach to extract heritable information from high-dimensional phenotypes and use it to holistically describe pattern variation in this system. We then used our phenotype data for a Genome Wide Association Study (GWAS) of color to identify the genetic architecture of a suite of color traits.

Our phenotypic and genomic results converge to show that color patterning in guppies is a combination of many heritable features, each with a partially overlapping genetic architecture. Unusually, our GWAS results suggest that copy number variation (CNV) is responsible for much of the variation in color in guppies, providing a novel mechanism for the origin and maintenance of male color diversity.

Artificial selection on orange coloration

Starting from an outbred laboratory population with large variation in color patterning, we created three replicate pairs of selection lines for reduced and increased amounts of orange coloration as a percent of total body area. Each male in the experiment (n = 3,229) had multiple photos taken from each side to track measurement error (n = 14,100). Using a series of neural networks, we performed image segmentation to separate the fish from the background, and to identify the orange and black coloration on the fish (Fig 1A). In addition to orange, xanthophores also create the less frequent yellow color patches, which we include in our orange measurements. We then warped images to a common reference shape based on placed landmarks to enable fine-scale color mapping (*9*). Combined with a full pedigree, this dataset allowed us to trace the inheritance of color patterns across four generations (Fig 1B). While some body areas are almost always pigmented (Fig 1C), color is rare in most places on the male body plan, giving each male a unique pattern.

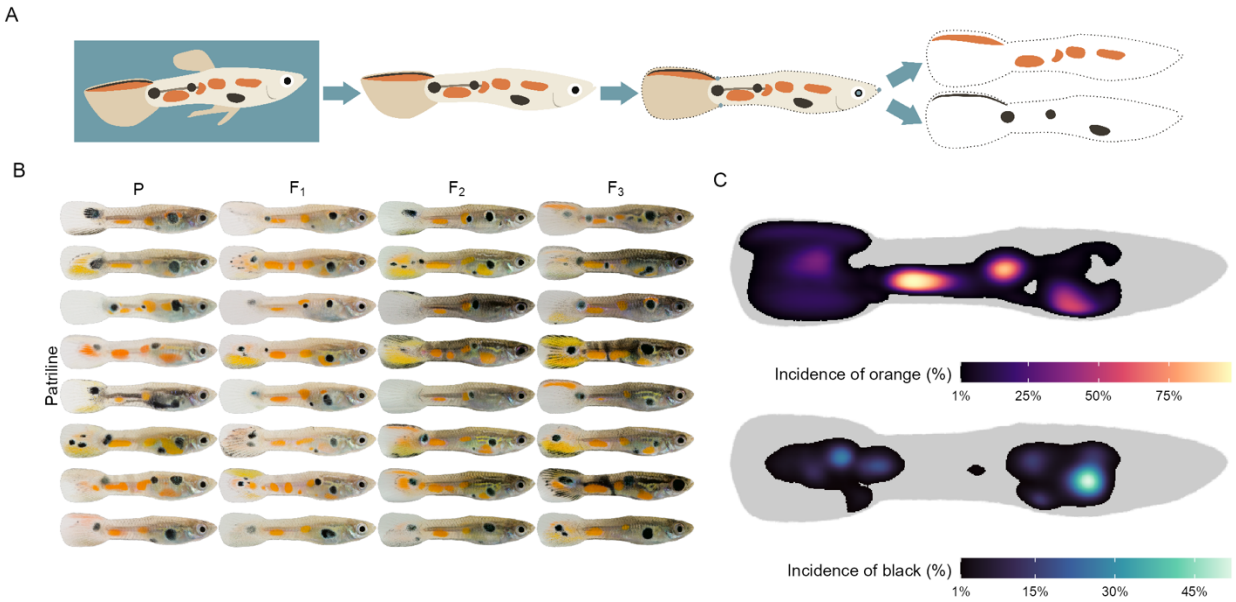

Figure 1: Quantification of pattern variation. A) Overview of the phenotyping pipeline. From each photo, the fish is extracted, the body is aligned to a common reference shape using landmarks, and the position of orange and black color is extracted. B) Randomly selected examples of color inheritance along patrilines. Images on the same row belong to the same patriline, and columns are successive generations of the selection experiment (both selection directions). C) The incidence of color across the guppy body among all males. Body positions where the incidence of color is less than 1% are colored grey.

The percent of orange color responded rapidly and strongly to selection (Fig 2A). After just three generations, up-selected males had more than double the amount of orange color compared to their down-selected counterparts (% up – % down in F_3 [95% credible interval]: 6.05 [5.67, 6.48]). We modeled the inheritance of black and orange color along the pedigree (*17*), separating autosomal, X-linked and Y-linked genetic effects, as well as influences due to the maternal and tank environments. The strong response in orange color to selection is consistent with its substantial heritability (narrow-sense h^2: 0.59, [0.50, 0.68], Fig S1). While orange and black ornaments share the same body plan, selection on orange nonetheless had a negligible effect on the amount of black coloration (up – down in F_3: -0.09 [-0.17, 0.01], Fig S3A). Although the amount of black color is also substantially heritable (h^2: 0.67 [0.53, 0.80], Fig S2), the amount of the two colors is inherited largely independently as evidenced by their low genetic correlations ($r_{autosomal}$: 0.07 [-0.15, 0.26], Fig S4). Although previous work on other

82 populations (*8*, *14–16*) has identified strong Y-linkage, our estimates of Y effects are low ($h^2_{\text{Y-linked}}$
83 orange: 0.03 [0.00, 0.09], black: 0.04 [0.00, 0.08], and instead the genetic variation for the proportion of
84 orange and black color on the body has an autosomal and, to a lesser extent, X-linked origin (Figs
85 S1&S2).

86 Our selection regime affected the incidence of orange color at nearly all positions on the body, with
87 effect sizes increasing with each successive generation of selection (Fig 2B). The strength and direction
88 of the effects were spatially heterogeneous. In the F_3 generation, up-selected males were approximately
89 5x more likely to have orange color at any particular position in the tail or caudal fin (posterior to the
90 gonopodium). The strongest effects were located close to the pectoral fin and gills, where up-selected
91 males were more than 100x as likely to have orange color on the ventral side, while surprisingly, they
92 were more than 100x *less* likely to be orange dorsally (although this dorsal color was much less

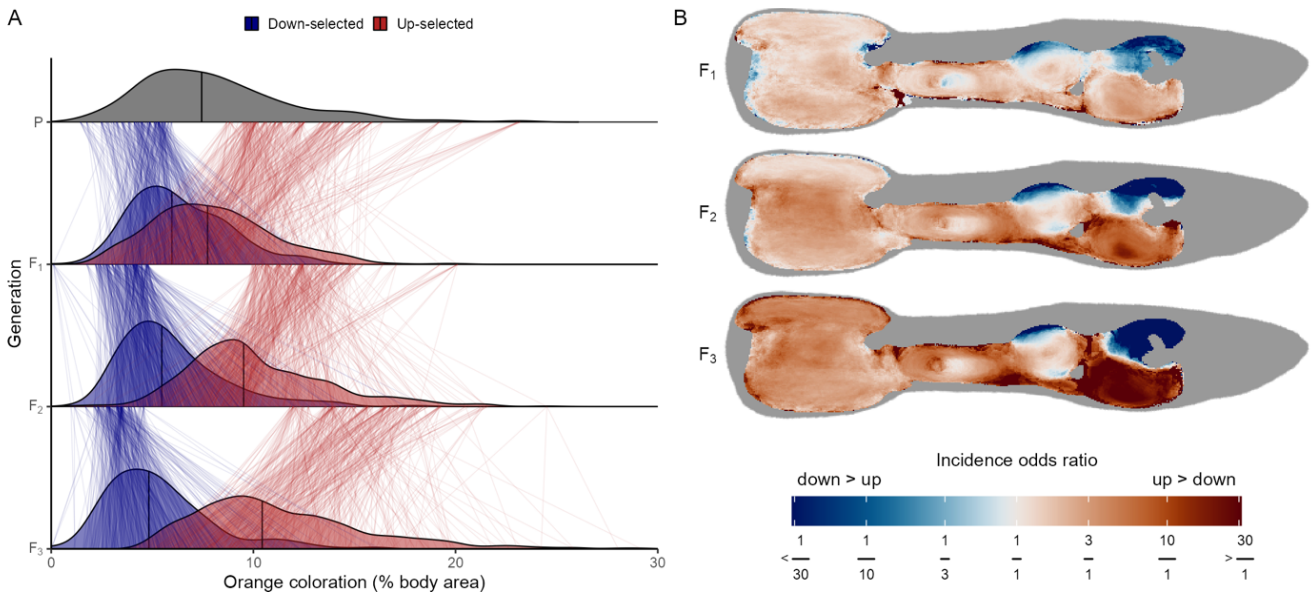

Figure 2: Orange color responds rapidly to selection. A) Density plots show the distribution of the percent of orange coloration per generation and selection regime. Thin lines between generations connect fathers to their sons. Thick lines inside the densities show the median value of color area. B) Heatmaps illustrating the effect of selection across the body. Each heatmap cell is colored by the log odds ratio (as estimated by a generalized linear mixed model), illustrating the relative odds that a male has orange color at that location. Body positions where the incidence of orange color is less than 1% are colored grey.

prevalent overall, Fig 1C). The response against the direction of selection at some locations, and correlated local changes in black color (Fig S3B), illustrate that elements of the color pattern are genetically linked.

To investigate whether other traits were also co-selected in our selection lines, we looked at changes in behavior and life history, since selection on embryonic neural crest cells has resulted in changes in these traits in other vertebrate systems (*18*, *19*). Guppy males show off their colors during characteristic sigmoid display behavior, where they curve their body into an S-shape, quiver, and swim laterally in front of females (*20*, *21*). Using males from the F_3 generation, we evaluated the effects of our selection regime on male sexual behavior. In a standard no-choice test with a non-receptive female, males from the up-selected lines performed both more (short displays: ratio up/down = 1.74, z = 2.15, p = 0.031, long displays: up/down = 1.84, z = 2.28, p = 0.022) and longer (up/down = 1.9, z = 2.44, p = 0.015) displays to the female (Fig S5). In addition, they spent more time following the female (up/down = 1.9, z = 2.44, p = 0.015, Fig S6), and performed more attempts at coercive sneak copulations (up/down = 1.99, z = 2. 09, p = 0.037), suggesting the more colorful males were 1.7-2x more sexually active overall (Fig S5). Males did not show changes in body size or tail size (standard length in mm, up – down in F_3: -0.36 [-0.84, 0.12], tail length: 0.10 [-0.21, 0.43], tail area mm^2: 0.019 [-2.5, 2.2], Fig S7), nor did selection alter the fecundity of females (F_2 offspring per brood, down-selected: 7.74, up-selected: 7.79, ratio up/down: 0.99 [0.87, 1.12]) or the time between pairing and the first brood (F_2, up - down in days: -1.23 [-3.4, 0.97], fig S8).

Localized heritability, ornaments, and patternspace

While the quantity of orange and black coloration are important to female choice (*5*, *22*), male patterning is largely inherited as discrete spots and stripes at fixed body positions (*9*, *14–16*). To understand the spatial structure of color inheritance, we modeled the heritability of the presence of color separately for each body location (Fig 3), confirming the fine-scale heritability of color patterning. In many places the localized heritability is high (> 0.8), much higher than the heritability of the total amount of color. Decomposing the genetic variance into autosomal and sex-linked components shows that the genetic architecture is highly spatially heterogeneous. For example, orange color in the top of the tail fin and black color ventrally of the dorsal fin were strongly X-linked, while both colors near the pectoral fin showed a large Y-linked component. This overlapping patchwork of genetic architecture generates the complexity of the color pattern.

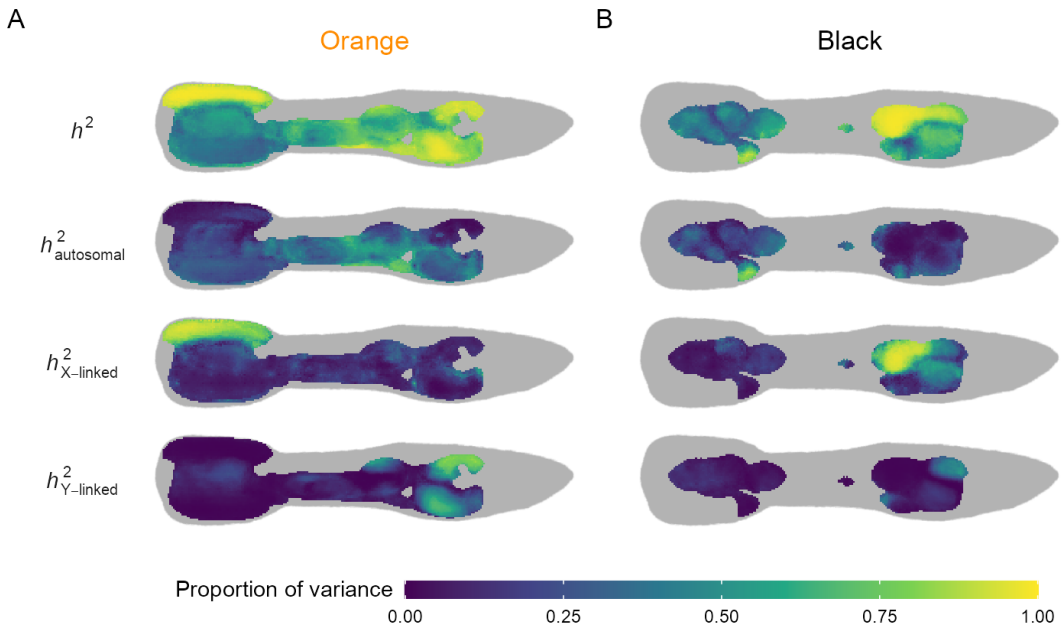

Figure 3: The localized heritability of color is high, but the architecture is heterogeneous. The narrow-sense heritability of the presence of orange (A) and black (B) color on the guppy body. For each heatmap cell, a Bayesian animal model was used to estimate the contribution of additive genetic and environmental factors. Heritabilities are expressed as a proportion of the between-individual phenotypic variance. The autosomal, X-linked, and Y-linked heritability add up to the total heritability. Body positions where the incidence of color is less than 1% are colored grey.

We defined seven orange (Fig 4) and eight black ornaments (Fig S9), based on the incidence of color (Fig 1C) and the localized genetic architecture (Fig 3). As expected, the incidence of all ornaments is heritable. In addition, their size is also heritable for all but one ornament (O3). All orange ornaments responded to selection on the total amount of orange, either in their incidence, their size or both (Fig 4C & 4D). Concordant with the localized analysis of inheritance, we find that the ornaments each have their own characteristic combination of autosomal, sex-linked and environmental causes. This can also be seen from the low correlations between many different ornaments with autosomal or X-linked

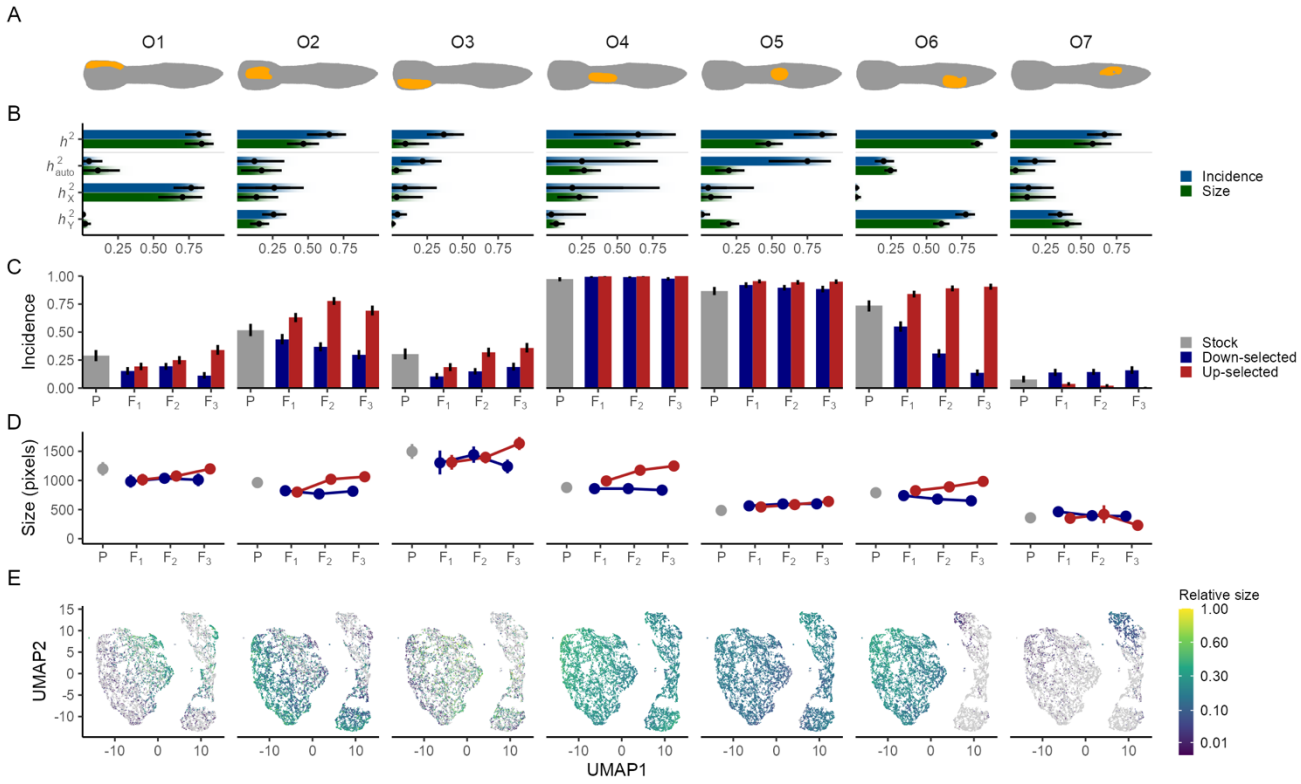

Figure 4: Orange ornaments are heritable and their incidence and size responded to selection. A) Pictograms of seven orange ornaments. B) Heritabilities of the incidence and size (when present) of each ornament. Dots and lines reflect point estimates and 95% credible intervals, and the gradient bars show the cumulative posterior density. C&D) Effect of selection on the incidence and size of orange ornaments. Bars and points represent means, with error bars showing 95% bootstrapped confidence intervals. X-axes show consecutive generations. E) Pattern space encodes variation in incidence and size of ornaments. Points are the location of individuals in pattern space. Axes are the UMAP reduced representation of five-dimensional pattern space. Individuals are colored by the size of their relevant ornament, expressed as a fraction of the largest observed size, or colored grey if they lack the ornament. Note the use of a logarithmic scale for ornament size.

architectures (Figs S10 & S11). In contrast, we observed strong Y-linked genetic correlations, consistent with a non-recombining Y chromosome. Within each ornament, however, the architecture of incidence and size were typically similar, which may indicate that additive genetic factors for ornament size also control its presence as a threshold trait.

These localized approaches will underestimate the true pattern diversity in the population if separate color elements are co-located. For example, some males exhibit large patches of color in the tail that do not neatly fit the three ornaments defined there (Fig S12). Similarly, they do not capture potential heritable differences in spot shape or color characteristics such as hue and saturation. To describe the orange and black patterns free from assumptions about developmental mechanism, we developed a novel high-dimensional phenomics approach using a deep neural network embedder which places the patterns within five-dimensional patternspace. Briefly, using triplet learning (*23*), these convolutional neural nets were trained to encode the heritable pattern variation of orange and black patterns (see Supplementary Methods). The networks are rewarded when they place patterns from related males closer together than those of unrelated males. As a result, these patternspaces are holistic summaries of the complex pattern variation among males. Patterns which are close in patternspace share heritable features, as can be observed when we map the presence and size of the ornaments onto this space (Fig 4E & S9E).

Orange patternspace is divided into two large clusters, differentiated by the presence of the highly heritable and Y-linked O6 ornament (Fig 4E). However, because the Y does not recombine, complete Y-linkage of color patterns results in discrete patterns associated with each patriline, which would be expected to form additional clusters, which we did not observe. Instead, the many heritable features combine into a continuous space of pattern variation consistent with high levels of autosomal and X-linked variation across the recombining portion of the genome. Our selection regime gradually separated the populations in patternspace over the generations (Fig S13). Nonetheless, as there are

many routes to increase or reduce the amount of orange, pattern variation is largely maintained within the selection lines among succeeding generations.

Mapping color pattern to the genome

We selected 300 males from the F_3 generation for short-read whole genome resequencing, sampling across all families and across patternspace to capture a wide variety of patterns. The guppy Y-chromosome is highly diverse (*24*), and using a male reference genome with one Y haplotype will create reference bias for all other Y haplotypes. However, the high degree of similarity between the X and Y for homologous regions (*25*, *26*) ensures that Y-linked reads will map to the X assembly. We therefore aligned our reads to the guppy female reference genome (*27*), which avoids reference bias to any particular Y haplotype. After variant calling and filtering, we performed multivariate GWAS separately for orange and black patternspace, and the absence/presence of orange and black ornaments. In addition, we verified associations using the reference-free *k*-mer based GWAS approach (*28*) (data not shown).

Consistent with the complex genetic architecture of the phenotypes, we found many regions of strong association with orange and black pattern across the genome (Fig 5A). Highly significantly-associated variants span the entirety of linkage group (LG) 12, the sex chromosomes, likely due to strong linkage across this region. Given the low differentiation between the X and Y for homologous regions (*24*, male:female coverage at LG12:21-26Mb = 0.986), most reads from the Y chromosome nonetheless map to the X chromosome in the female reference genome, and variants on LG12 represent a combination of pseudo-autosomal, X-linked and Y-linked variants (*25*). Ornament level GWAS (Figs 5B, S14 & S15) confirmed that ornaments with strongly sex-linked inheritance are associated most with LG12, that specific ornaments within the same biochemical color pathway are encoded through partially

176 overlapping suites of loci (Figs S16 & S17) and that the patternspace GWAS (Fig 5A) is largely a

177 composite of these individual architectures.

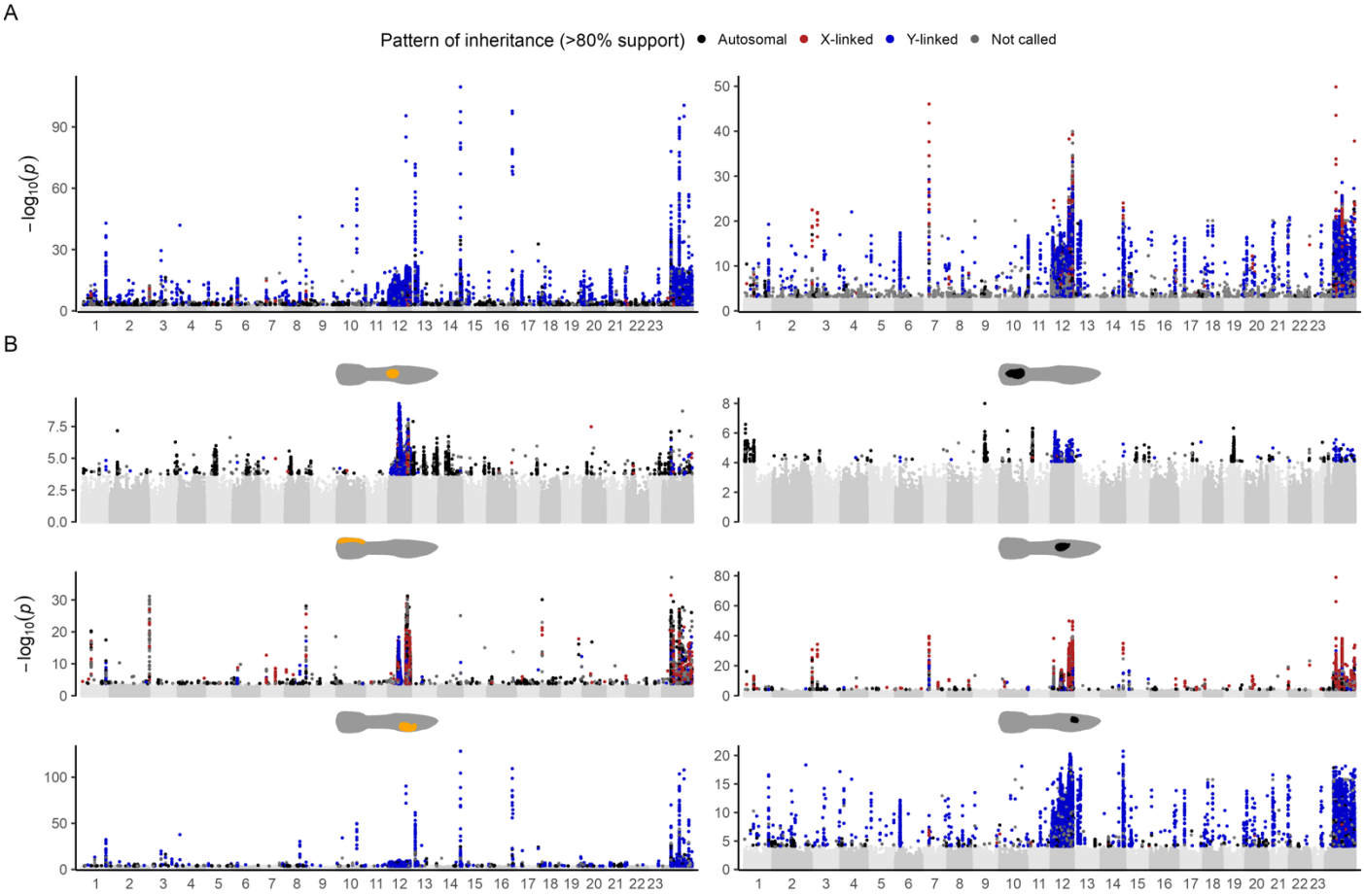

Figure 5: Manhattan plots of genomic associations with orange and black color. A) Results of multivariate GWAS on position in orange (left) and black (right) patternspace. Points represent SNPs and small indels, with their genomic location on the x-axis, and the p-value of the association on the y-axis. Numbers along the x axis denote linkage groups, with unplaced scaffolds plotted on the right-hand side. Significant associations (5% FDR) are colored by their inferred pattern of inheritance, whereas non-significant associations are colored in alternating shades of grey. B) GWAS results for the association with the presence/absence of select ornaments: O5, O1, and O6 (left), and B1, B5 and B8 (right). All ornaments shown in Figs S14 & S15.

178 In addition, we observed peaks of associated variants on nearly all autosomes. Strikingly, many of these

179 regions showed elevated coverage and heterozygosity, suggesting reads from copy number variants

180 (CNVs, Fig 6). Given recent work that identified CNVs spanning autosomes and the Y chromosome in

181 natural guppy populations (*29*) and the role of sex-linked variation in this system, we hypothesized that

reads from the Y chromosome regions that are not homologous to the X could map to these autosomal regions, representing CNVs spanning multiple genomic locations. We tested this conjecture by comparing the likelihood of autosomal, X- or Y-linked segregation of the variants in these regions based on our pedigree (Figs 5 & 6). Close to a third of significant variants which mapped to the autosomes showed sex-linked inheritance (orange pattern: 66 X-linked & 1,523 Y-linked out of 4,841 called variants; black pattern: 98 & 1,223 out of 4,056; Figs S18 & S19), confirming the involvement of CNVs with sex-linked copies. These sex-linked variants have much stronger associations with patternspace than the two-thirds which are autosomally inherited (Fig 5A). Consistent with the genetic correlations from our quantitative genetic analyses, sex-linked variants are shared much more frequently among traits than autosomal variants.

One possible explanation for the abundance of Y-linked variants in our GWAS is that they are all strongly linked to one or a few causal loci of large effect which control the Y-linked components of the color traits. To test this, we performed principal component analysis on the variants associated with orange pattern and a Y-linked inheritance pattern. If these loci have significant associations with orange pattern due to strong linkage to the same few alleles, we expect these variants to cluster into clear haplotypes that are strongly associated to color. Instead, we identify four putative Y-haplogroups with substantial variation within each haplogroup (Fig S20), and which only explain a small amount of color variation compared to individual variants (Figs 6E & S21). The fully non-recombining region of the Y chromosome is relatively small (*26*), and the majority of the chromosome recombines with the X exceedingly rarely (*30*). Although these rare X-Y recombination events might explain the variation without our four Y-haplogroups, this would also lead to expected X and Y segregation of SNPs. We therefore suggest that our data are more consistent with a substantial amount of Y diversity in our population.

204 The locus most strongly associated with orange pattern mapped to LG14 (an autosome), with many
205 significant variants in a 35kb region that are inherited in a Y-linked manner (Fig 6C), suggesting these
206 variants represent fixed differences between the autosomal region and its copies on the Y-chromosome.
207 Consistent with this scenario, we observed highly elevated coverage consistent with multiple Y-linked
208 copies in males, and a reduced coverage for females (Fig 6B). The gene located in this region
209 (LOC103476393) is uncharacterized in the annotation but has 72% sequence identity with *TeximYa* from
210 the related Southern platyfish (*Xiphophorus maculatus*). Copies of *Teximon* have also been found on the Y-
211 chromosome of the closely related *Poecilia parae* (*31*), suggesting duplication of *Teximon* to the Y-

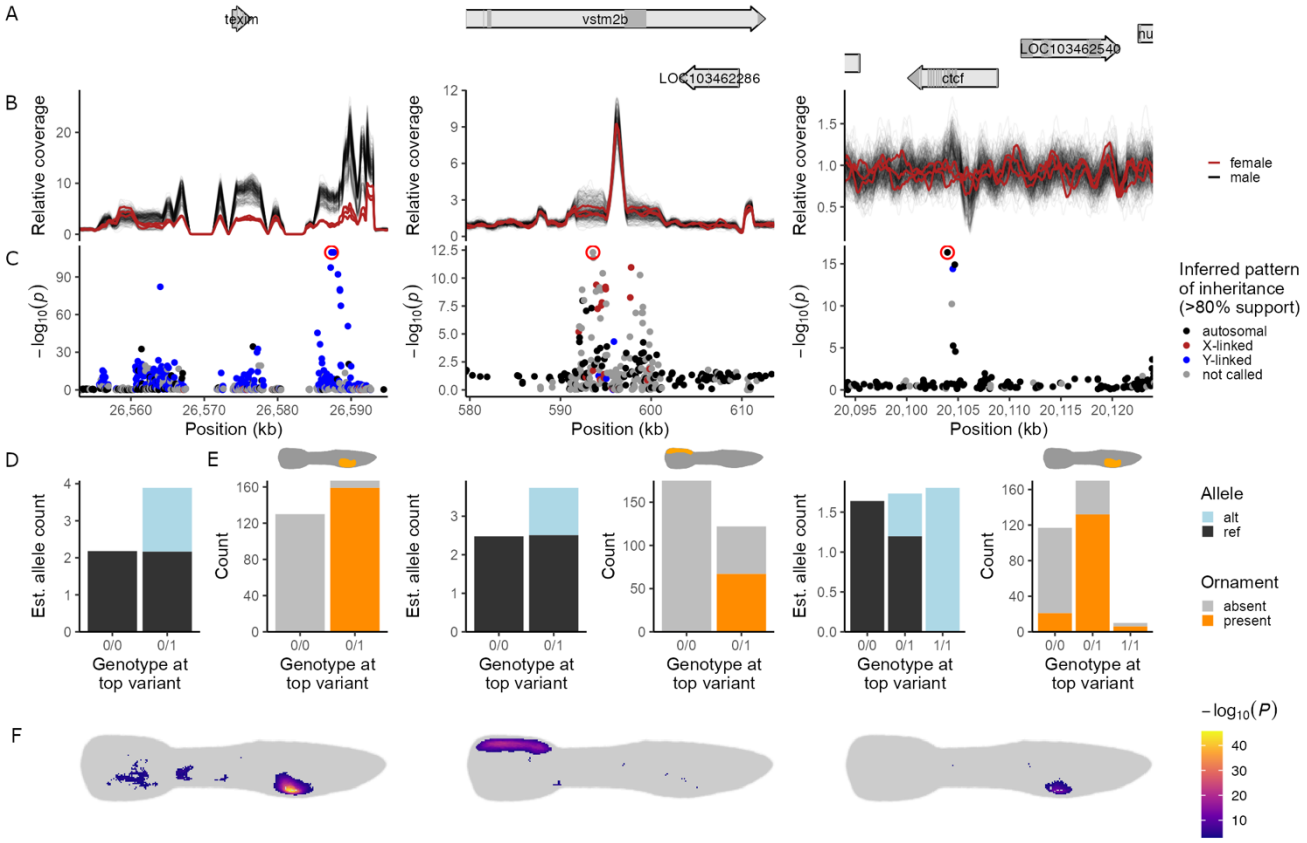

Figure 6: Examples of a Y-linked, X-linked and autosomal GWAS peak. A) Gene tracks, with shaded regions indicating exons. B) Relative coverage (1x = genome wide sample average) across the region for 297 males (this study) and 3 females (*64*), calculated in moving windows of 1000bp and a distance of 100bp. C) P-values for the GWAS association with orange color pattern. Variants are colored by their likely source based on pedigree information, with ambiguous variants colored grey (AIC weight < 80%). A red circle indicates the top variant used in panels D&E. D) The median estimated number of alleles per genotype and allele, calculated as half the median relative coverage at the top variant. E) Association of the top variant with the most associated orange ornament (O6, O1 and O6, from left to right). F) Localized effect of the top SNP on the incidence of orange coloration across the body. P-values are adjusted for genome-wide relatedness, and p-values > 0.001 are not shown.

chromosome is common in this clade. The most strongly associated variant in this region is located downstream of this *Texim* copy, and almost perfectly predicts the presence of the Y-linked ornament O6 (Fig 6C) while it is more weakly associated with the presence of O2 and the size of O4 (Fig 6D). Coverage for most of this region is elevated five to ten-fold and heterozygous individuals have increased coverage compared to individuals that are homozygous reference (Fig 6D).

Other regions show a similar pattern of CNV, but the additional reads originate from the X-chromosome instead. For example, a region on LG3 contains significant variants of both autosomal and X-linked inheritance, and the top variant is strongly predictive of the presence of the X-linked ornament O1. Also here, heterozygotes have increased coverage suggesting that X-linked CNVs are associated with this ornament. The duplicated region is intragenic, spanning a large exon of the gene *vstm2b*, a transmembrane protein with unknown function.

Across most peaks, similar to the two examples above, the genotype at the top variant is strongly related to the coverage. Since the variants mark both allelic variation and gene dose, we cannot differentiate the role of this sex-linked structural variation. It is notable, however, that the genotype with increased coverage encodes the presence of ornaments in almost all cases, suggesting an increase in dose is associated with greater color.

Finally, many smaller GWAS peaks are not associated with sex-linked variation, illustrating that the autosomal genetic component is polygenic with many loci of small effect. For example, a significant locus on LG3 is inherited autosomally, and lacks increased coverage. Six variants show an association with orange pattern, and fall in the gene *ctcf*, which is involved in regulating gene expression and chromatin architecture. Individuals that were homozygous reference at this locus were less likely to present ornament O6.

Discussion

The remarkable variation in male guppy coloration has made them a model for studies of female preference (*2*, *3*) and the interaction of sexual and natural selection (*4*, *32*). Male patterns in many populations have been shown to exhibit strong patterns of Y-linkage (*8*, *14*, *16*). This Y-linkage complicates detailed analysis of the genetic architecture of male color variation, as fine-scale genetic mapping requires recombination. Here we used a population with comparatively low levels of Y-linkage for color variation (*9*) to dissect the detailed genetic architecture for male color variation, using a combination of high-resolution phenotyping via neural nets, controlled pedigrees, and GWAS.

Our population has shown a rapid response to artificial selection for other complex traits (*33*–*35*), suggesting significant underlying genetic variation. Consistent with this, we observe substantial variation in male color (Fig 1) and a rapid response to artificial selection for increased and decreased orange coloration in all our replicate selection lines (Figs 2, 4 & S13). Male color has previously been shown to respond to artificial selection in other populations (*7*, *36*, *37*), and consistent with this, we observe high heritability (Figs 3 and 4) for both total color area and specific color ornaments.

One might expect that if black is epistatic to orange, selection to increase the area of the fish with orange coloration would reduce the total black area. That is not the case, as we observe little change in black area throughout the selection experiment but do see modest localized shifts in black color (Fig S3), more consistent with the repulsion of developing xanthophores and melanophores during color development (*38*).

We then used whole genome sequencing for 300 males from the F_3 generation, sampled to maximize their distribution within color-space to perform GWAS for multiple color traits (Figs 5 and 6). Interestingly, genes previously identified as key to melanophore formation in guppies, *colony-stimulating factor 1 receptor a* (also called *fms*), *kit ligand a* (*kita*) (*18*, *39*) and *adenylate cyclase 5*

(*adcy5*) (*40*), were not implicated in our GWAS (Fig S22). This suggests that although these loci are fundamental and necessary in the development of color cells, they do not contribute substantially to the variation in color pattern we observe in our population.

In contrast to melanin, carotenoids are not synthesized in vertebrates de novo, but rather collected from dietary intake and modified prior to deposition (*41*). This mode of color development is hypothesized to make carotenoid-based coloration a key mediator of honest sexual signaling of male quality (*1*, *42*, *43*). Consistent with this, males from selection lines with greater orange area exhibited greater sexual vigor (Fig S4 & S5), though we did not observe any correlated changes in female life history traits. The behavioral response to selection on color may be the result of pleiotropic changes to neural crest cells, which play a central role in both pigmentation and neurological development (*18*, *19*).

We might expect genes associated with carotenoid metabolism in other vertebrates to play a role in orange coloration in guppies. A key gene identified in red coloration of birds, cytochrome P450 locus CYP2J19 (*44*, *45*), lacks a reciprocal ortholog in teleost fish. Aldehyde dehydrogenase family 1 member A1, associated with red carotenoid coloration in lizards (*46*), is also not implicated in our GWAS. Instead, the region most strongly associated with orange color has high 72% sequence identity with *Texim*. Although the functional role of *Texim* remains unclear, it is thought to encode an esterase/lipase (*47*), which are important in carotenoid modification (*48*, *49*) and therefore may play a role in orange coloration.

Similarly, we do not find support for a large haplotype on LG1, which has been previously been indirectly implicated in guppy color variation in another population (*50*). Instead, our results suggest a far more complicated genetic architecture for color pattern. For both black and orange color, we observe specific ornaments encoded through partially overlapping suites of loci (Figs S16 & S17). Moreover, the architecture is heavily influenced by CNVs, although it is challenging to differentiate between gene dose

effects, with more copies of a gene associated with greater color, and allelic variation, with some copies associated with specific patterns. This aspect of the genetic architecture of guppy color is particularly interesting in that it might be expected to help maintain male phenotypic color variation more effectively than allelic variation in single-copy genes. It has been a long-standing mystery how the remarkable variation in male color is maintained against the eroding forces of genetic drift, selection and sweeps. Although female mate preferences for rare male patterns can be expected to preserve some male patterning variation (*2*, *10*, *11*), it is difficult to envisage how this would be sufficient to maintain the extensive variation observed in guppy populations, many of which formed with significant bottlenecks and founder effects.

The fact that we observe CNVs associated with color spanning autosomes and the sex chromosome may help to explain recent observations of variation in the extent of Y-linkage for color in wild populations (*51*, *52*). Although the size of the fully non-recombining region of the Y chromosome is relatively small (*25*, *26*), there is evidence that it can accumulate substantial recent duplications of genes from the remainder of the genome (*29*). If this process involves coloration loci and varies across populations, it is easy to envisage how the association between the Y chromosome and color variation could differ, even among closely related populations. It may also suggest that the low-levels of Y-linkage we observe in our population, originally collected from the high predation region of the Quare River, Trinidad, may be observed in other natural populations that either have lower rates of duplication to the Y, or lower levels of Y-duplicate retention. Finally, our data suggests that the Y-linked regions that do contribute to color in our population are surprisingly diverse.

This Y diversity could potentially lead to biased mapping and variant calling if we had used a male reference genome, as other Y haplotypes would suffer reduced mapping rates. To avoid this, we used a female reference genome. However, the sequence similarity between homologous regions of the X and Y chromosomes (*24*, *26*) ensures that Y-linked reads from this region will map to the X assembly.

Consistent with this, we identified substantial numbers of Y-linked SNPs segregating along patrilines in this region (Fig 5), indicating that Y-linked reads map effectively to the X chromosome.

Taken together, our results present a critical link between the extraordinary variation in male guppy coloration and the genome that encodes it. The fine-scale genetic architecture of color that we reveal presents an exciting opportunity for future molecular analyses of sexual selection dynamics and a critical point of comparison for future studies of the genetic architecture of color in other populations.

Acknowledgements

We thank Lengxob Yong for sharing insights on guppy photography. We thank Ben Sandkam, Ben Furman, David Metzger, Lydia Fong, Yuying Lin, Christina Hodson, and James Lewis for help with animal husbandry and valuable discussions, and Tom Booker for advice and comments on an earlier draft. Yuying Lin contributed the female coverage data. Funding was provided by a Canada 150 Research Chair, NSERC and an ERC grant (680951) to JEM.

Author contributions

Conceptualization: WvdB, AC-L & JEM, Methodology: WvdB, Formal analysis: WvdB & AC-L, Investigation: WvdB, JJS, VSG, LMS, MC-C, AC-L & JEM, Writing – Original Draft: WvdB & JEM, Writing – Review & Editing: WvdB, JJS, VSG, LMS, MC-C, AC-L & JEM, Visualization: WvdB, Supervision: JEM, Project administration: JJS, Funding acquisition: JEM.

Data and code availability

Code is available at https://github.com/Ax3man/vdBijl_etal_2024_GuppyColorPatterns. Data will be deposited upon

Materials and methods

Fish and animal husbandry

Our study population are descendants of guppies that were captured in Trinidad in 1998 and subsequently maintained in large, outbreeding stock populations to maintain genetic diversity, and males show large diversity in their ornamentation. 240 females for the parental generation (P) were randomly sampled as juveniles from our three stock populations and maintained as virgins until sexual maturity. 300 males for the parental generation were sampled as adults from the stock populations.

Fish were kept in 1.4 l tanks in three flow-through systems, with each experimental replicate in a separate system. Water was maintained at 25 °C, and lights were on a 12:12h cycle. Fish were fed daily with a mix of live brine shrimp and tropical fish micro pellets (Hikari, Japan), with immature fish fed an additional meal on weekdays of frozen daphnia and blood worms.

Experimental procedure and selection

Each replicate was started using 100 males, evenly sampled across the three stock populations. We quantified the amount of orange coloration for each male (see *Color pattern extraction and quantification*, below), and selected the 30 males with the largest and 30 males with the smallest total orange area to form paired up- and down-selected lines. For the P generation, these males were then randomly paired with females. To increase our statistical power to detect sex-linked variation, we paired 10 males of each line with two females each to generate half siblings, and 20 males with a single female each, creating a partial half-sib breeding design. For subsequent generations, we selected the 30 males with greatest orange area in up-selected lines, and the 30 males with least orange for down-selected lines. Additionally, we increased the strength of selection by selecting on females. Since females do not express orange coloration, we used an animal model to estimate breeding values (see *Quantitative genetics,* below). We then selected the females with greatest and least breeding value (40 for each

category), incorporating uncertainty by ranking across draws from the posterior distribution. To avoid a rapid loss of genetic variation, and to limit the selective advantage of males paired with two females, we further limited our selection to include a maximum of three sons from each sire, and three daughters from each dam.

For the males matched with two females, females were kept in separate tanks, and the male was moved between females each week. We collected broods from the up- and down-selected lines until we had 90 broods per generation per replicate. 93.3% of paired males and 89.3% of paired females successfully sired offspring, resulting in an average of 1.46 broods per sire, and 1.10 broods per dam. Having >1 brood per pair allowed us to estimate the magnitude of brood effects.

Broods were collected within a few days of birth to avoid infanticide and moved to their own tank. To maintain similar developmental rates, broods larger than ten individuals were randomly reduced to ten. Broods were checked three times per week for signs of male maturation (first signs of gonopodium growth), and males were moved to a separate tank to avoid sibling mating. The tanks with male brood members were then queued for phenotyping after visual conformation of sexual maturity (fully developed color pattern), and a minimum age of 60 days. After phenotyping (see *Color pattern extraction and quantification*, below), males were housed in individual tanks to maintain their identities.

The three replicates were set up staggered in time, so that one replicate could be phenotyped while the others were breeding and maturing. Fish were only marked with their individual IDs, blinding the experimenters as to which line individuals belonged to throughout experimental procedures and phenotyping (except when setting up the next generation of breeding pairs).

Animal photography and calibration

We (WvdB & JJS) captured photos of male color patterns using a Canon EOS Rebel T7i (Canon, Japan) with Canon EF 100mm f/2.8 Macro USM lens (Canon, Japan). All photos were captured using identical

camera settings, at an aperture of f/11, an exposure time of 1/320s, an ISO of 800 and an approximate distance of 35-40 cm, and we captured a color standard *in situ* before each photography session (ColorChecker Passport Photo 2, X-rite, USA). Photos were captured in RAW format, then color corrected in Adobe Lightroom (Adobe, USA), see *Supplemental methods*.

The photarium (photo tank) was placed on a pedestal covered with matte black felt, inside a 30 x 60 x 30 cm photo box. The walls and top of the box were constructed of opaque white plastic, to minimize the influence of external lights. In the top, directly above the pedestal, we mounted 2 Neewer NL660 LED panels with white diffusers, with a color rendering index of >= 96 (Neewer, China).

We photographed both sides of every fish, and for 99.9% of fish we had at least three photos, with the replicate photos allowing us to parse measurement error from asymmetry. We analyzed a total of 14,100 photos, or an average of 4.37 photos per fish.

Color pattern extraction and quantification

After color correction, we used a custom pipeline to analyze the images. The pipeline consists of deep neural networks for image segmentation and landmark placement, and geometric morphometrics for image alignment. To be able to phenotype fish during the selection procedure, when we still had little data available to train the models, we adopted a semi-autonomous strategy. We used an interactive script to phenotype fish, which prompted the experimenter (WvdB) to visually check the output of each analysis step, and correct manually when the model prediction was incorrect. We then intermittently updated model weights with the growing number of manually annotated examples to improve model performance, gradually reducing the need for manual intervention throughout the experiment. The pipeline consisted of these five steps:

Step 1: We first performed image segmentation to separate the fish from the background. We excluded the gonopodium and dorsal fin from the extracted fish; since their size is not consistent on camera, they

394 are difficult to segment due to their transparency, and they do not exhibit ornamentation in our
395 population. We used a convolutional neural net with a Unet (*53*) architecture, implemented in the *unet*
396 R package (*54*), with six layers in the encoder, 10 filters in the first convolution, a dropout of 0.25 and
397 with binary cross-entropy as the loss function. Using the segmentation mask, we then cropped and
398 rotated the fish to an image of dimension [800 x 300 x 4], (three color channels and the segmentation
399 mask).

400 Step 2: Next, we further segmented the fish image with two additional Unet models, to extract the
401 carotenoid and melanic coloration respectively. Both used four layers in the encoder, 12 filters in the
402 first convolution, a dropout of 0.5 and a Dice loss function.

403 Step 3: To be able to directly compare regions of the guppy body, we performed image alignment. We
404 trained a convolutional neural net to place four landmarks on the fish: in the center of the eye, on the
405 tip of the snout, and on the dorsal and ventral extremes of the boundary between the caudal peduncle
406 and the tail fin. Instead of predicting the landmark coordinates directly, which worked poorly, the
407 landmarks were represented as a stack of four images, each having a point (with Gaussian blur) at one
408 landmark location. The model was then trained to predict these landmark images, taking the extracted
409 fish from Step 1 as input. The model first has three convolutional layers, followed by three
410 deconvolutional layers, to transform the three color channels into four heatmaps of landmark
411 probability (Table S1). We then selected the highest activation on each output channel as the predicted
412 landmark coordinates.

413 Step 4: Treating the four landmarks from Step 3 as fixed, we added sliding semi-landmarks
414 algorithmically. We first mirrored all images of the left side of the fish, then found all pixels on the
415 boundary of the segmentation mask from Step 1, which is the outline of the fish. These pixels were
416 ordered into a continuous curve by treating the connection between points as a Travelling Salesman

Problem. Using the fixed landmarks from Step 3, we split this curve into three: a) the outline from the tip of the snout, along the back, to the dorsal attachment of the caudal fin, b) the outline of the caudal fin, dorsal to ventral, and c) from the ventral attachment of the caudal fin to the tip of the snout. Along each of these curves we placed 50 evenly spaced semi-landmarks.

Step 5: Using the fixed landmarks from Step 3 and sliding landmarks from Step 4, we use Generalized Procrustes analysis to generate a consensus shape using package *geomorph* (*55*). Using thin-plate spline transformation, we then warped our fish images to the consensus shape with package *Morpho* (*56*). This warping is applied to the segmented fish from Step 1, and the segmented ornamentation from Step 2. Since these are continuous transformations, we then rasterized the warped output by taking color averages along a grid, resulting in images of dimension [500 x 140 x 4].

By comparing the number of pixels in the extracted fish mask from Step 1, and the number of pixels in the extracted carotenoid and melanin masks from Step 2 (i.e. before warping), we calculate the amount of coloration as a percentage of the body area. For use in our selection paradigm, we calculated the mean across multiple photos of each side of each fish, and then the mean across the sides.

For manual segmentation for Step 1, we annotated the fish' outline with splines using the *StereoMorph* package (*57*). For manual color segmentation in Step 2, we used the free and fuzzy select tools in the GNU Image Manipulation Program (GIMP). For black segmentation, we only selected distinct color patches of concentrated pigmentation, which are always present. We excluded the various facultatively expressed darker areas, sometimes referred to as "fuzzy black" (*8*, *21*).

Quantifying effects of selection

We quantified the effect of selection on the amount of orange and black coloration using Bayesian linear mixed models (LMMs) using *brms* (*58*, *59*). We modeled the amount of color as a percentage of the body area as the dependent variable, with fixed effects of generation, selection direction and their

interaction, and a random intercept per generation nested within experimental replicate. We then calculated the contrast in marginal means between up- and down-selected fish of the F_3 generation. We used the same modelling approach for the effect of selection on life history parameters, except that we modelled fecundity using the negative binomial distribution. We report effects in the last generation (where effects are strongest) from these models, based on contrasts calculated using *emmeans* (*60*). In addition, we estimated the effect of selection on orange and black color per body location (Fig 2B & S3) using independent binomial generalized linear mixed models with *lme4* (*61*), using the same model structure, and the presence/absence of orange as the dependent variable.

Male sexual behavior

We assessed the sexual behavior of 126 male offspring from the F3 generation (63 from each selection direction, evenly split across the replicate lines). We isolated males upon early indications of sexual maturity (first signs of gonopodial development), then at around three months tested their sexual behaviors using a no choice test with nonreceptive females, a standard for studying male sexual behavior in poecilids. Behavioral trials took place in a 47 cm diameter arena, with fish transfer followed by a 5-minute acclimation to minimize stress and a 15-minute observation using a webcam at 1080p and 30 fps. We analyzed the recorded videos to quantify male sexual behaviors. We utilized idTracker (*62*) for positional data during each trial. Trials where females exhibited receptivity or where fish showed signs of stress were excluded, leading to a final dataset of 95 individuals. Statistical analysis on behavioral differences between high and low orange males used generalized linear mixed models implemented in *glmmTMB* (*63*), with behavioral metrics as dependent variables, selection direction, male body size, and female body size as fixed effects, and replicate line as random effect. Behavioral counts were modelled using the negative binomial distribution, while for time spent following we used the Gaussian distribution with log link function.

Ornaments

We defined areas of the fish as ornaments manually, based on the visible spatial structure in the incidence of color and the localized genetic architecture (Figs 1C & 3). We then overlayed these areas on the extracted color patterns from each photo, and counted the number of pigmented pixels within each area. We scored an ornament as "absent" (ornament size = 0) if < 10% of the ornament area was pigmented. This limit was chosen based on the bimodal distribution of the number of pixels, as in some cases a few pixels from a neighboring ornament spilled over into other areas.

We determined the distribution of each male fish in patternspace using using triplet learning (*23*), where we trained convolutional neural nets (see Supplementary Methods).

Quantitative genetics

Estimating of quantitative genetic (QG) parameters for the amount of orange and black color was performed by MCMC sampling of Gaussian animal models implemented in *Stan* (*64*) with *brms* (*58*, *59*). Additive genetic variance-covariance matrices were calculated from the pedigree using *nadiv* (*65*), with the *S* matrix for X-linked effects assuming no global dosage compensation (*26*). Y-linked genetic variances were estimated by including patriline as a group level effect. Similarly, we included dam identity to estimate maternal effects, included brood identity to capture shared environmental effects between siblings, and individual identity to estimate the remaining environmental influence, all as group level effects. We included the side of the fish, nested in individual identity as a group level effect to estimate the variance due to asymmetry, and included the residual variance to estimate measurement error. For all variances, including the residual variances, we estimated their correlation among the two colors. We used default non-informative priors for all parameters.

For the QG heatmaps (Fig 3), we estimated separate animal models for each bin, estimating orange and black colors separately. We used the same model structure as the model above, now with a Bernoulli

error structure. We also removed the maternal effect, as the clutch and maternal effects are similar and their magnitudes are small. Since estimating these parameters independently thousands of times using MCMC is prohibitively computationally expensive, we used an approach that makes use of the fact that the QG estimations will be similar between neighboring bins. To limit the number of models, we reduced the dimensions of the color pattern images by a factor of two (250 x 70 bins or pixels), and only ran models for bins with an incidence of at least 1%. We then performed model fitting in two rounds. First, we fit animal models for the bins with x- and y-coordinates divisible by five. For these models, we used four chains, with 500 warmup iterations and 1500 sampling iterations per chain, and uninformative StudentT(3, 0, 5) priors on the intercept and variance components. In a second step, we then used the output of these models to fill in the bins between this five-by-five grid. These models only used two chains of 500 warmup iterations and 500 sampling iterations, but were seeded with initial parameter values and step sizes that were the average of the closest nine models from Step 1, weighted by their inverse distance. Similarly, we set normal priors for the intercept and variance components with the mean (also weighted by inverse distance) and standard deviation of those parameters of the closest nine models.

For ornament heritability, we used similar models to the amount of orange and black color, but used hurdle-lognormal models instead to jointly estimate the variance components for the incidence and size (when present) of the ornaments. Given the very small maternal effects on total color, we did not include that parameter here. We specified an uninformative logistic(0, 5) prior on the hurdle parameter, and a StudentT(3, 0, 5) parameter on the standard deviations of the group level effects, with otherwise default priors.

For the pairwise correlations across ornaments, we used the Gaussian approximation and fitted the multivariate animal model on individual-level means using the restricted maximum likelihood method

509 from *sommer* (*66*). Given the small magnitude of brood effects from the full Bayesian animal models for
510 each ornament, we did not include that effect here.

511 ## Learning of patternspace

512 We devised a deep learning approach to map images of guppies onto a "patternspace". Our objective
513 was to capture the heritable components of color patterns by placing images of related guppies more
514 proximately in this patternspace compared to those of unrelated males. Our method is predicated on
515 the "triplet loss learning" paradigm (*23*).

516 The deep learning architecture was designed to process images of dimensions 250x70x3, with the last
517 dimension being color channels. Our model, a Convolutional Neural Network (CNN), had a series of
518 layers that successively compress the images to lower dimensions. Specifically, we used separable
519 convolutional layers with a kernel size of 3x3 and *relu* activation, followed by a max pooling layer,
520 repeating this four times. Each convolutional layer had double the filters of the previous, starting at 8
521 filters. After the fourth pooling layer, we flattened the output to a dense layer of size 8, and then a
522 second dense layer of the embedding dimension. Finally, since we wanted to achieve a dense
523 representation, we did not use L1 normalization, but a batch normalization layer to normalize
524 activations to unit variance. Embeddings are obtained at this normalization layer.

525 The essence of our method hinges on the generation and use of "triplets". A triplet comprises an anchor
526 image (a random male), a positive image (of a related male), and a negative image (of an unrelated
527 male). Unrelated males had a coefficient of relatedness *r* of 0, while for related males *r* was at least 1/8.
528 During training, each image is passed through the CNN described above and the triplet loss function is
529 applied. The objective was to reduce the distance (in the embedding space) between the anchor and
530 positive images, while increasing the distance between the anchor and negative images, governed by a
531 margin.

We trained for 50 epochs using a batch size of 128 images. At each epoch, we randomly generated 5,000 triplets. We randomly allocated 20% of individuals to the validation set, from which we generated 500 triplets per epoch to track model performance. Moreover, learning rate schedules were implemented to adjust the learning rate across epochs, with specified rates of 10^{-4}, 10^{-5}, and 10^{-6} at epochs 0, 30, and 40 respectively. This scheduling ensured a faster convergence initially, with fine-tuning during the latter stages of training.

We evaluated the number of embedding dimensions by training the model at one to eight dimensions, then chose five dimensions, since the model accuracy for the validation sample stopped increasing above five. After training, we used the CNN to embed all 14,100 images. All analyses use the five embedding dimensions while for visualization we performed dimension reduction using UMAP (*67*), which aims to preserve the local neighborhood structure of the data, as implemented in R package *uwot* (*68*).

Genetic sampling and whole genome sequencing

To maximize power for the genetic mapping of color traits, we sampled 50 fish from each selection line (N = 300) for whole genome sequencing (WGS). To maximize genetic and phenotypic variation in our sample, and therefore power, we sampled males from each family with offspring in generation F_3, and sampled males with the most/least carotenoid coloration in up/down-selected lines respectively. This meant we sampled one son from each family, with some families contributing a second son until we reached the desired 50 males.

We euthanized males via submersion in ice water followed by decapitation and stored their heads in 95% ethanol. DNA was extracted from half a head using Qiagen Dneasy blood & tissue kits (Qiagen, USA). Samples were then sequenced on four lanes of Illumina NovaSeq 6000 S4 PE150 to an average depth of 10x per individual. One individual was not included because the library failed. We checked the

identity of samples by visually comparing the genome-wide relatedness (GRM) with the pedigree-based relatedness (A) and excluded two samples which did not match, leaving 297 samples for analysis.

Genome-wide association analysis

We first trimmed the adapters using *Trimmomatic*, and then mapped the reads to the reference using *bwa mem* using default mapping parameters. We marked PCR duplicates using GATK's *MarkDuplicates*. We then called variants using *bcftools mpileup* where we downgraded the mapping quality of reads containing mismatches with *–adjust-MQ 60*, and set a minimal mapping quality using *–min-MQ 30*, followed by variant calling using the consensus caller *bcftools call*. We then performed variant filtering, and dropped sites with a QUAL score < 30, and sites where more than 20% of individuals had a depth < 5, or > 20% of individuals had a GQ score < 10. Additionally, we filtered out sites with a major allele frequency < 10% or a missingness > 5%.

We performed multivariate GWAS by running GEMMA (*69*) on each of the 5 axes of patternspace, using the centered genomic relatedness matrix (GRM) calculated from the variants mapping to the autosomes. We then calculated Z-scores and combined them to obtain multivariate p-values using CPASSOC (*70*). For univariate ornament GWAS, we also used GEMMA with likelihood ratio tests.

Coverage statistics were calculated using *samtools depth*, with a window size of 1000bp and a window distance of 100bp. We additionally calculated coverage for sequencing data from 3 females from the same population taken from (*71*) (NCBI BioProject accession PRJNA858015, sequenced at ~30x coverage), which were re-analyzed using the identical pipeline used for the males from the current study. We controlled the false discovery rate (FDR) by estimating *q*-values (*72*) separately for the orange and black patternspace GWAS. For ornament GWAS, we estimated the q-values jointly across the ornaments, but separately per color. FDR is controlled to 5% within each of these four sets of tests. We compared the overlap in associated variants between traits using the *ComplexUpset* package (*73*).

We performed principal component analysis to detect Y-haplogroups using *irlba* (*74*). We assigned the haplogroups using hierarchical clustering on the Euclidian distance matrix of the first 20 principal components using *hclust*. Package *GMMAT* (*75*) was used to estimate the effect of variants across locations on the body while controlling for the GRM (Fig 6F), using the score method and Gaussian approximation.

Inference of variant inheritance pattern

The inheritance pattern of variants implicated in the GWAS was estimated using animal models. We encoded the genotypes as doses of the alternative allele, and then fitted three models using *sommer* (*66*) with dose as the dependent variable. The three models included a random effect for the autosomal, X-linked or Y-linked covariance, respectively, as described in *Quantitative genetics*. For each model we calculated Akaike's Information Criterion (AIC) and their AIC weight (i.e. the relative likelihood) to compare between the three hypotheses. We called the inheritance of a variant if the relative likelihood exceeded 80%, labelling them "Not called" otherwise.

Software

Unless stated otherwise above, all analyses were performed in the R statistical environment (*76*).

References

1. J. F. Stephenson, M. Stevens, J. Troscianko, J. Jokela, The Size, Symmetry, and Color Saturation of a Male Guppy's Ornaments Forecast His Resistance to Parasites. *Am. Nat.* **196**, 597–608 (2020).
2. T. Potter, J. Arendt, R. D. Bassar, B. Watson, P. Bentzen, J. Travis, D. N. Reznick, Female preference for rare males is maintained by indirect selection in Trinidadian guppies. *Science* **380**, 309–312 (2023).
3. A. E. Houde, Mate choice based upon naturally occurring color-pattern variation in a guppy population. *Evolution* **41**, 1–10 (1987).
4. J. A. Endler, Natural Selection on Color Patterns in Poecilia reticulata. *Evolution* **34**, 76–91 (1980).
5. A. E. Houde, J. A. Endler, Correlated Evolution of Female Mating Preferences and Male Color Patterns in the Guppy Poecilia reticulata. *Science* **248**, 1405–1408 (1990).
6. D. J. Kemp, D. N. Reznick, G. F. Grether, J. A. Endler, Predicting the direction of ornament evolution in Trinidadian guppies (Poecilia reticulata). *Proc. R. Soc. B Biol. Sci.* **276**, 4335–4343 (2009).
7. M. Herdegen-Radwan, S. Cattelan, J. Buda, J. Raubic, J. Radwan, What do orange spots reveal about male (and female) guppies? A test using correlated responses to selection. *Evolution* **75**, 3037–3055 (2021).
8. R. Brooks, J. A. Endler, Direct and indirect sexual selection and quantitative genetics of male traits in guppies (Poecilia reticulata). *Evolution* **55**, 1002–1015 (2001).
9. J. Morris, I. Darolti, W. van der Bijl, J. E. Mank, High-resolution characterization of male ornamentation and re-evaluation of sex linkage in guppies. *Proc. R. Soc. B Biol. Sci.* **287**, 20201677 (2020).
10. K. A. Hughes, A. E. Houde, A. C. Price, F. H. Rodd, Mating advantage for rare males in wild guppy populations. *Nature* **503**, 108–110 (2013).
11. J. A. Farr, Male Rarity or Novelty, Female Choice Behavior, and Sexual Selection in the Guppy, Poecilia reticulata Peters (Pisces: Poeciliidae). *Evolution* **31**, 162–168 (1977).
12. D. M. Parichy, J. E. Spiewak, Origins of adult pigmentation: diversity in pigment stem cell lineages and implications for pattern evolution. *Pigment Cell Melanoma Res.* **28**, 31–50 (2015).
13. M. B. Toomey, C. I. Marques, P. M. Araújo, D. Huang, S. Zhong, Y. Liu, G. D. Schreiner, C. A. Myers, P. Pereira, S. Afonso, P. Andrade, M. A. Gazda, R. J. Lopes, I. Viegas, R. E. Koch, M. E. Haynes, D. J. Smith, Y. Ogawa, D. Murphy, R. E. Kopec, D. M. Parichy, M. Carneiro, J. C. Corbo, A mechanism for red coloration in vertebrates. *Curr. Biol.* **32**, 4201-4214.e12 (2022).
14. Ø. Winge, One-sided masculine and sex-linked inheritance inLebistes reticulatus. *J. Genet.* **12**, 145–162 (1922).
15. Ø. Winge, E. Ditlevsen, Colour inheritance and sex determination in Lebistes. *Heredity* **1**, 65–83 (1947).
16. C. P. Haskins, P. Young, R. E. Hewitt, E. F. Haskins, Stabilised heterozygosis of supergenes mediating certain Y-linked colour patterns in populations of Lebistes Reticulatus. *Heredity* **25**, 575–589 (1970).
17. L. E. B. Kruuk, Estimating genetic parameters in natural populations using the 'animal model.' *Philos. Trans. R. Soc. Lond. B. Biol. Sci.* **359**, 873–890 (2004).
18. D. M. Parichy, D. G. Ransom, B. Paw, L. I. Zon, S. L. Johnson, An orthologue of the kit-related gene fms is required for development of neural crest-derived xanthophores and a subpopulation of adult melanocytes in the zebrafish, Danio rerio. *Development* **127**, 3031–3044 (2000).
19. A. S. Wilkins, R. W. Wrangham, W. T. Fitch, The "Domestication Syndrome" in Mammals: A Unified Explanation Based on Neural Crest Cell Behavior and Genetics. *Genetics* **197**, 795–808 (2014).
20. N. R. Liley, Ethological Isolating Mechanisms in Four Sympatric Species of Poeciliid Fishes. *Behav. Suppl.* **1**, 1–197 (1966).

21. A. Houde, *Sex, Color, and Mate Choice in Guppies* (Princeton University Press, 1997).
22. R. Brooks, J. A. Endler, Female Guppies Agree to Differ: Phenotypic and Genetic Variation in Mate-Choice Behavior and the Consequences for Sexual Selection. *Evolution* **55**, 1644–1655 (2001).
23. F. Schroff, D. Kalenichenko, J. Philbin, "FaceNet: A unified embedding for face recognition and clustering" in *2015 IEEE Conference on Computer Vision and Pattern Recognition (CVPR)* (2015), pp. 815–823.
24. P. Almeida, B. A. Sandkam, J. Morris, I. Darolti, F. Breden, J. E. Mank, Divergence and Remarkable Diversity of the Y Chromosome in Guppies. *Mol. Biol. Evol.* **38**, 619–633 (2021).
25. A. E. Wright, I. Darolti, N. I. Bloch, V. Oostra, B. Sandkam, S. D. Buechel, N. Kolm, F. Breden, B. Vicoso, J. E. Mank, Convergent recombination suppression suggests role of sexual selection in guppy sex chromosome formation. *Nat. Commun.* **8**, 14251 (2017).
26. I. Darolti, A. E. Wright, B. A. Sandkam, J. Morris, N. I. Bloch, M. Farré, R. C. Fuller, G. R. Bourne, D. M. Larkin, F. Breden, J. E. Mank, Extreme heterogeneity in sex chromosome differentiation and dosage compensation in livebearers. *Proc. Natl. Acad. Sci.* **116**, 19031–19036 (2019).
27. A. Künstner, M. Hoffmann, B. A. Fraser, V. A. Kottler, E. Sharma, D. Weigel, C. Dreyer, The Genome of the Trinidadian Guppy, Poecilia reticulata, and Variation in the Guanapo Population. *PLOS ONE* **11**, e0169087 (2016).
28. Y. Voichek, D. Weigel, Identifying genetic variants underlying phenotypic variation in plants without complete genomes. *Nat. Genet.* **52**, 534–540 (2020).
29. Y. Lin, I. Darolti, B. L. S. Furman, P. Almeida, B. A. Sandkam, F. Breden, A. E. Wright, J. E. Mank, Gene duplication to the Y chromosome in Trinidadian Guppies. *Mol. Ecol.* **31**, 1853–1863 (2022).
30. R. Bergero, J. Gardner, B. Bader, L. Yong, D. Charlesworth, Exaggerated heterochiasmy in a fish with sex-linked male coloration polymorphisms. *Proc. Natl. Acad. Sci.* **116**, 6924–6931 (2019).
31. B. A. Sandkam, P. Almeida, I. Darolti, B. L. S. Furman, W. van der Bijl, J. Morris, G. R. Bourne, F. Breden, J. E. Mank, Extreme Y chromosome polymorphism corresponds to five male reproductive morphs of a freshwater fish. *Nat. Ecol. Evol.* **5**, 939–948 (2021).
32. J. A. Endler, "Natural and sexual selection on color patterns in poeciliid fishes" in *Evolutionary Ecology of Neotropical Freswater Fishes* (Springer, The Netherlands, 1984)*Developments in Environmental Biology of Fishes*, pp. 95–111.
33. A. Kotrschal, B. Rogell, A. Bundsen, B. Svensson, S. Zajitschek, I. Brännström, S. Immler, A. A. Maklakov, N. Kolm, Artificial Selection on Relative Brain Size in the Guppy Reveals Costs and Benefits of Evolving a Larger Brain. *Curr. Biol.* **23**, 168–171 (2013).
34. S. Fong, B. Rogell, M. Amcoff, A. Kotrschal, W. van der Bijl, S. D. Buechel, N. Kolm, Rapid mosaic brain evolution under artificial selection for relative telencephalon size in the guppy (Poecilia reticulata). *Sci. Adv.* **7**, eabj4314 (2021).
35. A. Kotrschal, A. Szorkovszky, J. Herbert-Read, N. I. Bloch, M. Romenskyy, S. D. Buechel, A. F. Eslava, L. S. Alòs, H. Zeng, A. Le Foll, G. Braux, K. Pelckmans, J. E. Mank, D. Sumpter, N. Kolm, Rapid evolution of coordinated and collective movement in response to artificial selection. *Sci. Adv.* **6**, eaba3148 (2020).
36. A. E. Houde, Effect of artificial selection on male colour patterns on mating preference of female guppies. *Proc. R. Soc. Lond. B Biol. Sci.* **256**, 125–130 (1994).
37. G. L. Cole, J. A. Endler, Change in male coloration associated with artificial selection on foraging colour preference. *J. Evol. Biol.* **31**, 1227–1238 (2018).
38. M. Inaba, H. Yamanaka, S. Kondo, Pigment Pattern Formation by Contact-Dependent Depolarization. *Science* **335**, 677–677 (2012).
39. V. A. Kottler, A. Fadeev, D. Weigel, C. Dreyer, Pigment Pattern Formation in the Guppy, Poecilia reticulata, Involves the Kita and Csf1ra Receptor Tyrosine Kinases. *Genetics* **194**, 631–646 (2013).

40. V. A. Kottler, A. Künstner, I. Koch, M. Flötenmeyer, T. Langenecker, M. Hoffmann, E. Sharma, D. Weigel, C. Dreyer, Adenylate cyclase 5 is required for melanophore and male pattern development in the guppy (Poecilia reticulata). *Pigment Cell Melanoma Res.* **28**, 545–558 (2015).
41. A. H. Brush, Metabolism of carotenoid pigments in birds. *FASEB J.* **4**, 2969–2977 (1990).
42. G. E. Hill, J. D. Johnson, The Vitamin A–Redox Hypothesis: A Biochemical Basis for Honest Signaling via Carotenoid Pigmentation. *Am. Nat.* **180**, E127–E150 (2012).
43. G. F. Grether, J. Hudon, D. F. Millie, Carotenoid limitation of sexual coloration along an environmental gradient in guppies. *Proc. R. Soc. Lond. B Biol. Sci.* **266**, 1317–1322 (1999).
44. R. J. Lopes, J. D. Johnson, M. B. Toomey, M. S. Ferreira, P. M. Araujo, J. Melo-Ferreira, L. Andersson, G. E. Hill, J. C. Corbo, M. Carneiro, Genetic Basis for Red Coloration in Birds. *Curr. Biol.* **26**, 1427–1434 (2016).
45. N. I. Mundy, J. Stapley, C. Bennison, R. Tucker, H. Twyman, K.-W. Kim, T. Burke, T. R. Birkhead, S. Andersson, J. Slate, Red Carotenoid Coloration in the Zebra Finch Is Controlled by a Cytochrome P450 Gene Cluster. *Curr. Biol.* **26**, 1435–1440 (2016).
46. C. A. McLean, A. Lutz, K. J. Rankin, A. Elliott, A. Moussalli, D. Stuart-Fox, Red carotenoids and associated gene expression explain colour variation in frillneck lizards. *Proc. R. Soc. B Biol. Sci.* **286**, 20191172 (2019).
47. M. Tomaszkiewicz, D. Chalopin, M. Schartl, D. Galiana, J.-N. Volff, A multicopy Y-chromosomal SGNH hydrolase gene expressed in the testis of the platyfish has been captured and mobilized by a Helitron transposon. *BMC Genet.* **15**, 44 (2014).
48. A. Pérez-Gálvez, M. I. Mínguez-Mosquera, Esterification of xanthophylls and its effect on chemical behavior and bioavailability of carotenoids in the human. *Nutr. Res.* **25**, 631–640 (2005).
49. D. E. Breithaupt, A. Bamedi, U. Wirt, Carotenol fatty acid esters: easy substrates for digestive enzymes? *Comp. Biochem. Physiol. B Biochem. Mol. Biol.* **132**, 721–728 (2002).
50. J. R. Paris, J. R. Whiting, M. J. Daniel, J. Ferrer Obiol, P. J. Parsons, M. J. van der Zee, C. W. Wheat, K. A. Hughes, B. A. Fraser, A large and diverse autosomal haplotype is associated with sex-linked colour polymorphism in the guppy. *Nat. Commun.* **13**, 1233 (2022).
51. S. P. Gordon, A. López-Sepulcre, D. Rumbo, D. N. Reznick, Rapid Changes in the Sex Linkage of Male Coloration in Introduced Guppy Populations. *Am. Nat.* **189**, 196–200 (2017).
52. S. P. Gordon, A. López-Sepulcre, D. N. Reznick, PREDATION-ASSOCIATED DIFFERENCES IN SEX LINKAGE OF WILD GUPPY COLORATION. *Evolution* **66**, 912–918 (2012).
53. O. Ronneberger, P. Fischer, T. Brox, "U-Net: Convolutional Networks for Biomedical Image Segmentation" in *Medical Image Computing and Computer-Assisted Intervention – MICCAI 2015*, N. Navab, J. Hornegger, W. M. Wells, A. F. Frangi, Eds. (Springer International Publishing, Cham, 2015)*Lecture Notes in Computer Science*, pp. 234–241.
54. D. Falbel, K. Zak, unet: U-Net: Convolutional Networks for Biomedical Image Segmentation, version 0.1, RStudio (2023); https://github.com/r-tensorflow/unet.
55. E. K. Baken, M. L. Collyer, A. Kaliontzopoulou, D. C. Adams, geomorph v4.0 and gmShiny: Enhanced analytics and a new graphical interface for a comprehensive morphometric experience. *Methods Ecol. Evol.* **12**, 2355–2363 (2021).
56. S. Schlager, "Morpho and Rvcg – Shape Analysis in R" in *Statistical Shape and Deformation Analysis*, G. Zheng, S. Li, G. Szekely, Eds. (Academic Press, 2017), pp. 217–256.
57. A. M. Olsen, M. W. Westneat, StereoMorph: an R package for the collection of 3D landmarks and curves using a stereo camera set-up. *Methods Ecol. Evol.* **6**, 351–356 (2015).
58. P.-C. Bürkner, Advanced Bayesian Multilevel Modeling with the R Package brms. *R J.* **10**, 395–411 (2018).
59. P.-C. Bürkner, brms: An R Package for Bayesian Multilevel Models Using Stan. *J. Stat. Softw.* **80**, 1–28 (2017).

60. R. V. Lenth, *Emmeans: Estimated Marginal Means, Aka Least-Squares Means* (2023; https://CRAN.R-project.org/package=emmeans).
61. D. Bates, M. Mächler, B. Bolker, S. Walker, Fitting Linear Mixed-Effects Models Using lme4. *J. Stat. Softw.* **67**, 1–48 (2015).
62. A. Pérez-Escudero, J. Vicente-Page, R. C. Hinz, S. Arganda, G. G. de Polavieja, idTracker: tracking individuals in a group by automatic identification of unmarked animals. *Nat. Methods* **11**, 743–748 (2014).
63. M. E. Brooks, K. Kristensen, K. J. van Benthem, A. Magnusson, C. W. Berg, A. Nielsen, H. J. Skaug, M. Maechler, B. M. Bolker, glmmTMB Balances Speed and Flexibility Among Packages for Zero-inflated Generalized Linear Mixed Modeling. *R J.* **9**, 378–400 (2017).
64. B. Carpenter, A. Gelman, M. D. Hoffman, D. Lee, B. Goodrich, M. Betancourt, M. Brubaker, J. Guo, P. Li, A. Riddel, Stan: A Probabilistic Programming Language. *J. Stat. Softw.* **76** (2017).
65. M. E. Wolak, nadiv: an R package to create relatedness matrices for estimating non-additive genetic variances in animal models. *Methods Ecol. Evol.* **3**, 792–796 (2012).
66. C.-P. Giovanny, Genome assisted prediction of quantitative traits using the R package sommer. *PLoS ONE* **11**, 1–15 (2016).
67. L. McInnes, J. Healy, J. Melville, UMAP: Uniform Manifold Approximation and Projection for Dimension Reduction. arXiv arXiv:1802.03426 [Preprint] (2020). https://doi.org/10.48550/arXiv.1802.03426.
68. J. Melville, *Uwot: The Uniform Manifold Approximation and Projection (UMAP) Method for Dimensionality Reduction* (2023; https://CRAN.R-project.org/package=uwot).
69. X. Zhou, M. Stephens, Genome-wide efficient mixed-model analysis for association studies. *Nat. Genet.* **44**, 821–824 (2012).
70. X. Li, X. Zhu, "Cross-Phenotype Association Analysis Using Summary Statistics from GWAS" in *Statistical Human Genetics: Methods and Protocols*, R. C. Elston, Ed. (Springer, New York, NY, 2017; https://doi.org/10.1007/978-1-4939-7274-6_22)*Methods in Molecular Biology*, pp. 455–467.
71. Y. Lin, I. Darolti, W. van der Bijl, J. Morris, J. E. Mank, Extensive variation in germline de novo mutations in Poecilia reticulata. *Genome Res.* **33**, 1317–1324 (2023).
72. J. D. Storey, R. Tibshirani, Statistical significance for genomewide studies. *Proc. Natl. Acad. Sci.* **100**, 9440–9445 (2003).
73. M. Krassowski, ComplexUpset (2020). https://doi.org/10.5281/zenodo.3700590.
74. J. Baglama, L. Reichel, B. W. Lewis, *Irlba: Fast Truncated Singular Value Decomposition and Principal Components Analysis for Large Dense and Sparse Matrices* (2022; https://CRAN.R-project.org/package=irlba).
75. H. Chen, M. Conomos, D. Pham, *GMMAT: Generalized Linear Mixed Model Association Tests* (2023; https://CRAN.R-project.org/package=GMMAT).
76. R Core Team, *R: A Language and Environment for Statistical Computing* (R Foundation for Statistical Computing, Vienna, Austria, 2023; https://www.R-project.org/).

Supplemental methods

Color calibration

Fish were photographed while swimming in a photarium. For the P and F_1 generations, we used a glass photarium measuring 16 x 85 x 100 mm (internal length x width x height), with an approximate water level of 3 cm. For generations F_2 and F_3, we instead used a thin plastic 54 mm cuboid box with an internal sliding white wall. In this photarium (following (*74*)) the fish can be restricted to a very narrow area in the front by sliding the white wall forward. Since the change in photarium led to small changes in color characteristics, we performed color calibration to match the two setups. To this end, we photographed 15 fish with both methods, and extracted the fish from the images. We then generated look-up-tables (LUTs) by matching color quantiles from these images in Lab color space. Photographs from the new photorarium were then adjusted to match the old color profile using the LUTs prior to analysis.

Supplemental figures

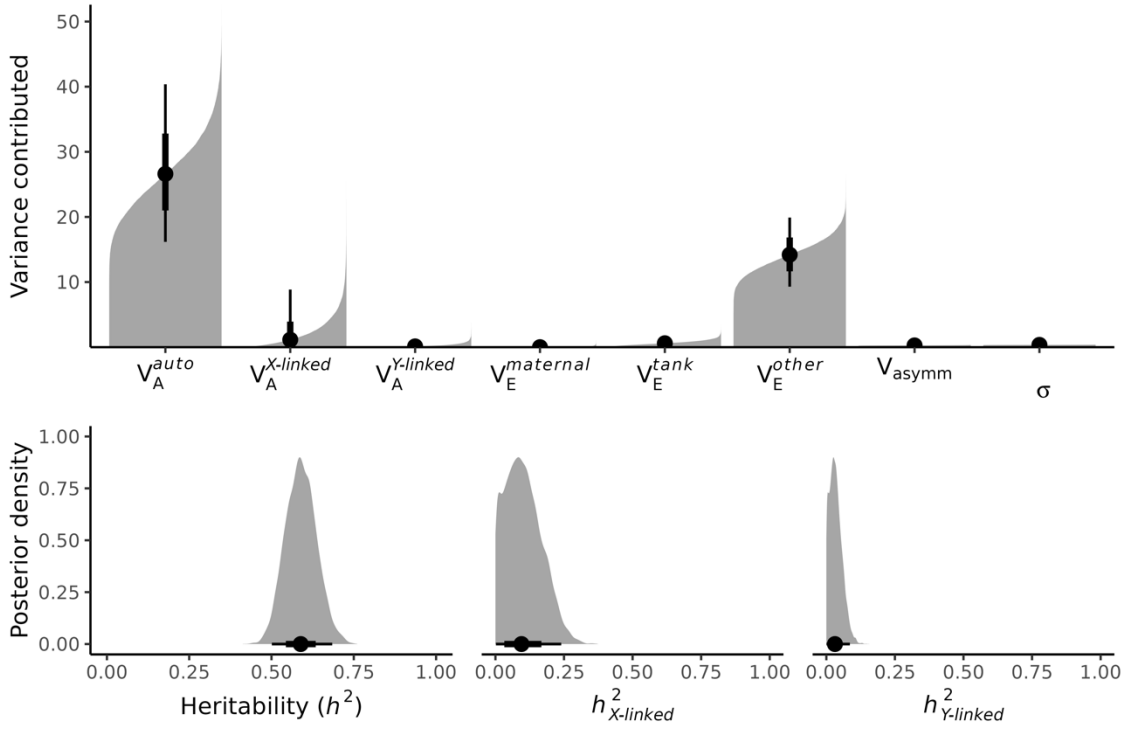

Figure S1: Variance components of total amount of orange color, as estimated by a Bayesian animal model. Top panel shows cumulative posterior density bar graphs, bottom panel shows posterior distributions. Posterior summaries are shown as posterior means (point) and 66% (thick lines) and 95% (thin lines) credible intervals.

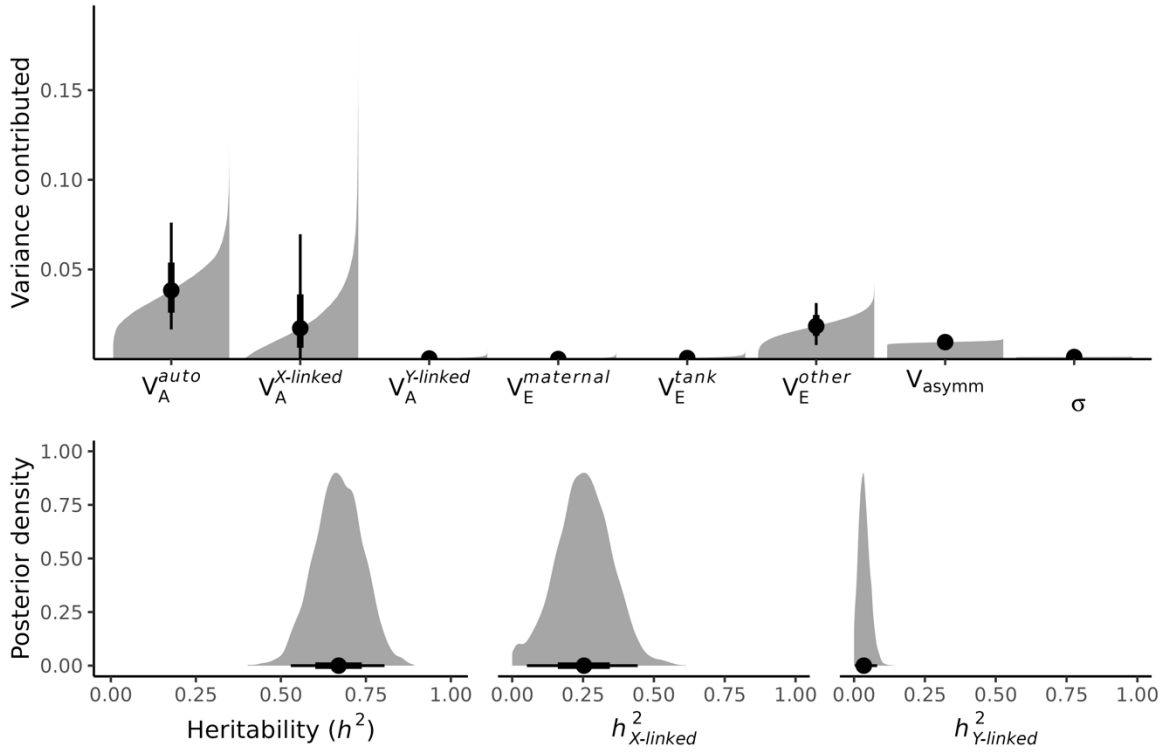

Figure S2: Variance components of total amount of black color, as estimated by a Bayesian animal model. Top panel shows cumulative posterior density bar graphs, bottom panel shows posterior distributions. Posterior summaries are shown as posterior means (point) and 66% (thick lines) and 95% (thin lines) credible intervals.

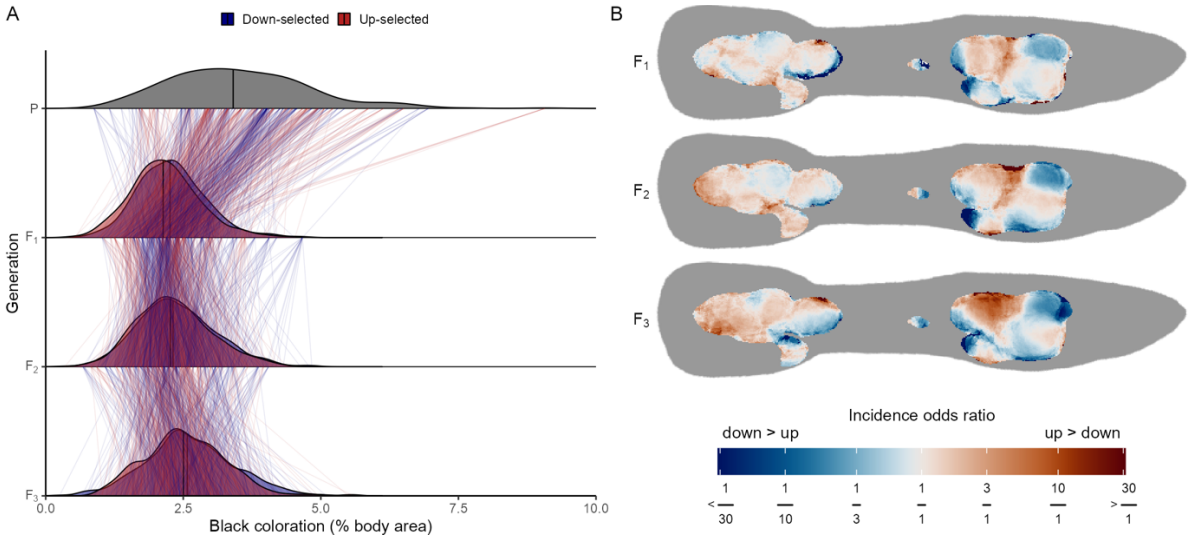

Figure S3: Correlated effects of selection on orange area on the incidence of black coloration. A) Density plots show the distribution of the percent of black coloration per generation and selection regime. Thin lines between generations connect fathers and sons. Thick lines inside the densities show the median value of color area. B) Heatmaps illustrating the effect of selection across the body. Each heatmap cell is colored by the log odds ratio (as estimated by a generalized linear mixed model), illustrating the relative odds that a male has black color at that location. Body positions where the incidence of black color is less than 1% are colored grey.

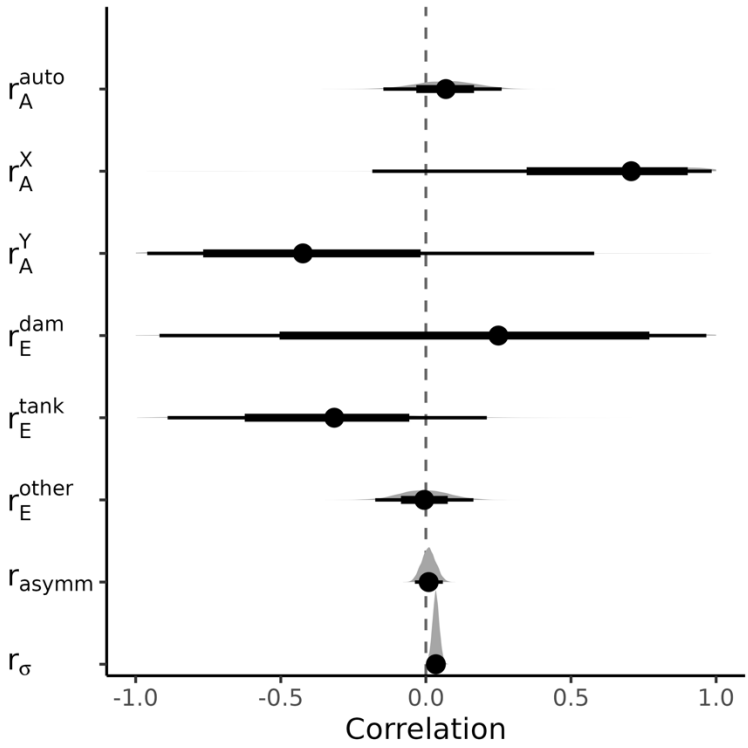

Figure S4: Posterior distributions of the correlation of orange and black variance components (Figs S1&S2). Posterior summaries are shown as posterior means (point) and 66% (thick lines) and 95% (thin lines) credible intervals.

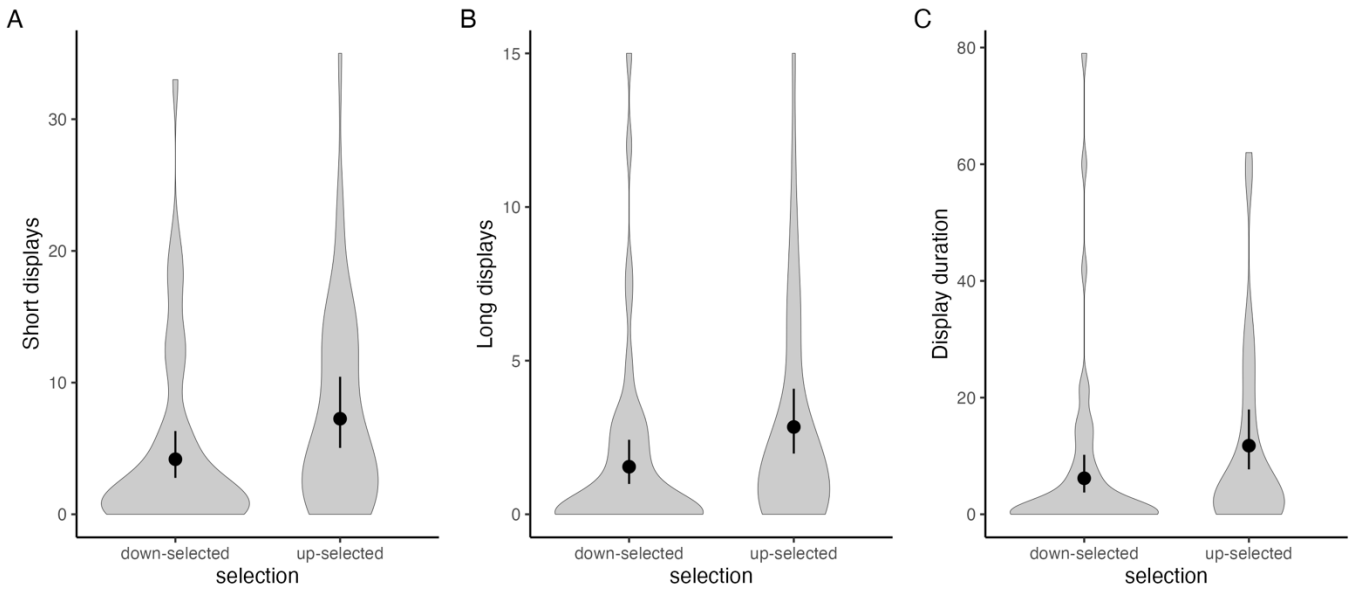

Fig S5: The effect of artificial selection for orange coloration on display behavior of male guppies. Comparison of a) frequency of short displays; b) frequency of long displays; and c) duration of display in down-selected (n = 46) and up-selected (n = 49) males from the F_3 generation. Violin plots show the kernel densities of observations, and point estimates and error bars show the point estimate and 95% confidence intervals for the groups means estimated by a linear mixed model.

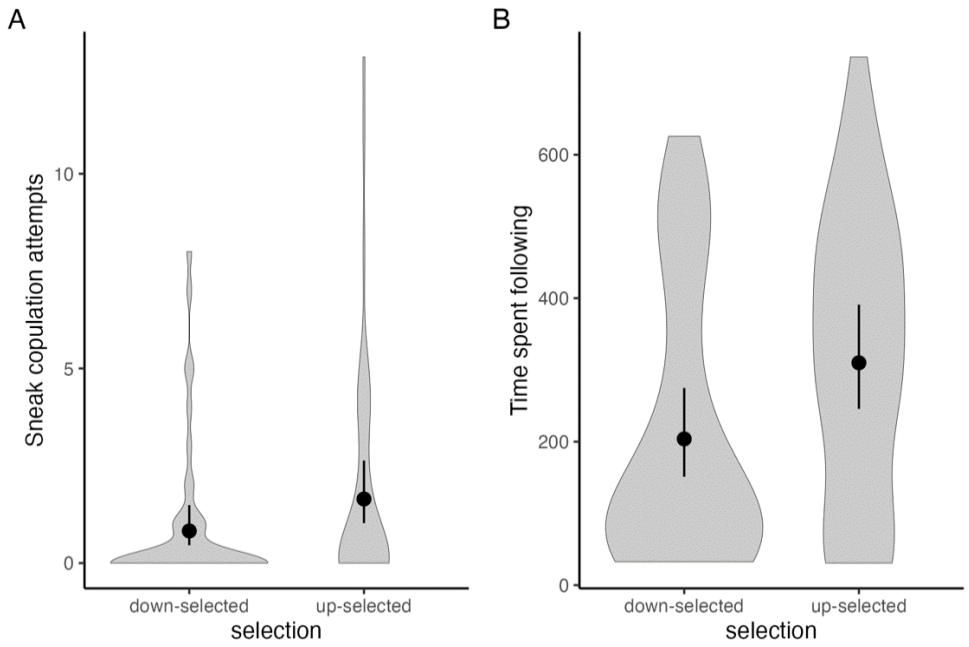

Fig S6: The effect of artificial selection for orange coloration on coercive sexual behavior of male guppies. Comparison of a) sneak copulation attempts and b) time spent following the female in of down-selected (n = 46) and up-selected (n = 49) males from the F_3 generation. Violin plots show the kernel densities of observations, and point estimates and error bars show the point estimate and 95% confidence intervals for groups mean as estimated by a linear mixed model.

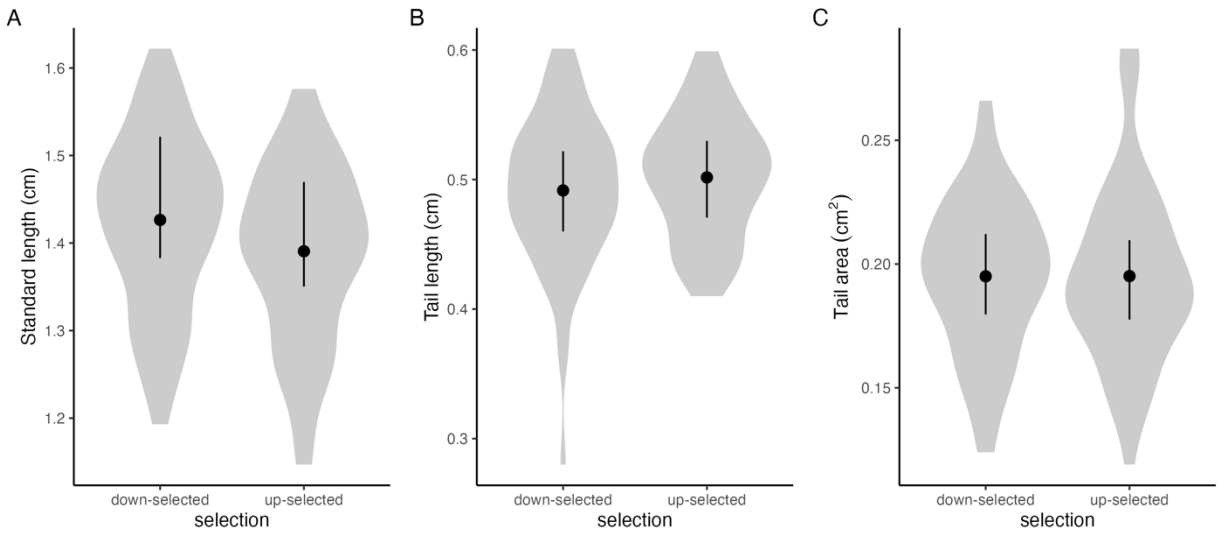

Fig S7: The effect of artificial selection for orange coloration on gross morphology of male guppies. Comparison of a) standard length b) tail length and c) tail area in male guppies following three generations of artificial selection for high (n = 62) and low (n = 63) proportion of orange. Violin plots show the kernel densities of observations while point estimates and error bars show the posterior median and 95% credible intervals for the groups means estimated by a linear mixed model.

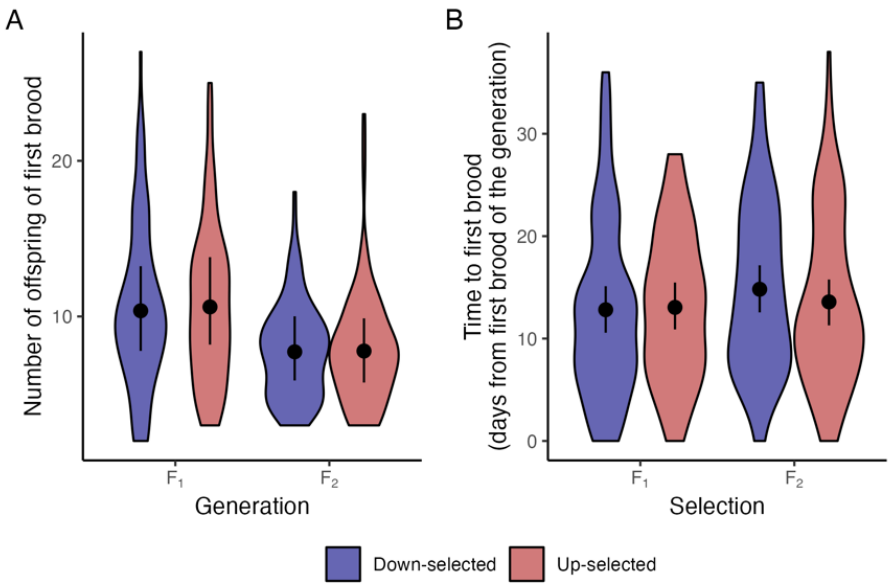

Fig S8: The effect of selection on orange coloration on life history parameters. A) shows the fecundity of females, as the number of offspring in their first brood. B) shows the time between pairing and the first brood (day 0 is the first brood of the generation). Violin plots show the kernel densities of observations while point estimates and error bars show the posterior median and 95% credible intervals for the groups means estimated by a linear mixed model.

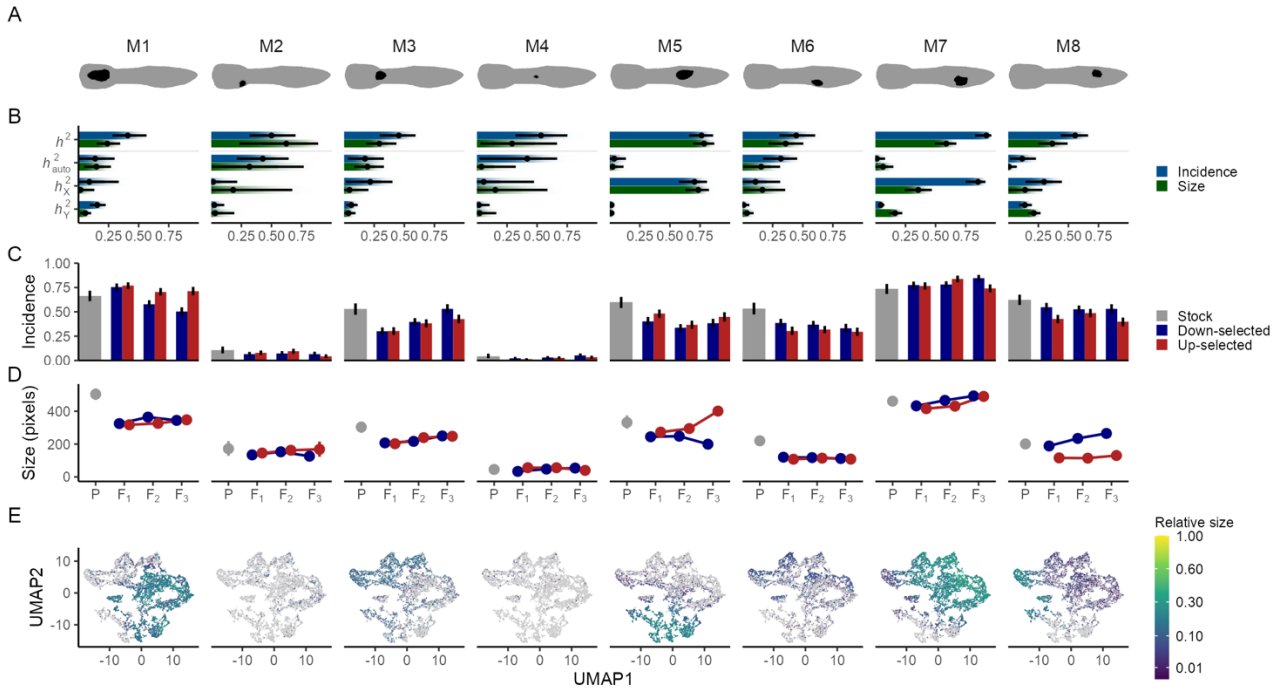

Fig S9: Black ornaments are heritable but responded only weakly to selection on orange color. A) Pictograms of eight black ornaments. B) Heritabilities of the incidence and size (when present) of each ornament. Dots and lines reflect point estimates and 95% credible intervals, and the gradient bars show the cumulative posterior density. C&D) Effect of selection on the incidence and size of black ornaments. Error bars show 95% bootstrapped confidence intervals, and points represent means. X-axes show consecutive generations. E) Ornaments in black pattern space. Points are the location of individuals in pattern space. Axes are the UMAP reduced representation of five-dimensional pattern space. Individuals are colored by the size of their relevant ornament, expressed as a fraction of the largest observed size, or colored grey if they lack the ornament. Note the use of a logarithmic scale for ornament size.

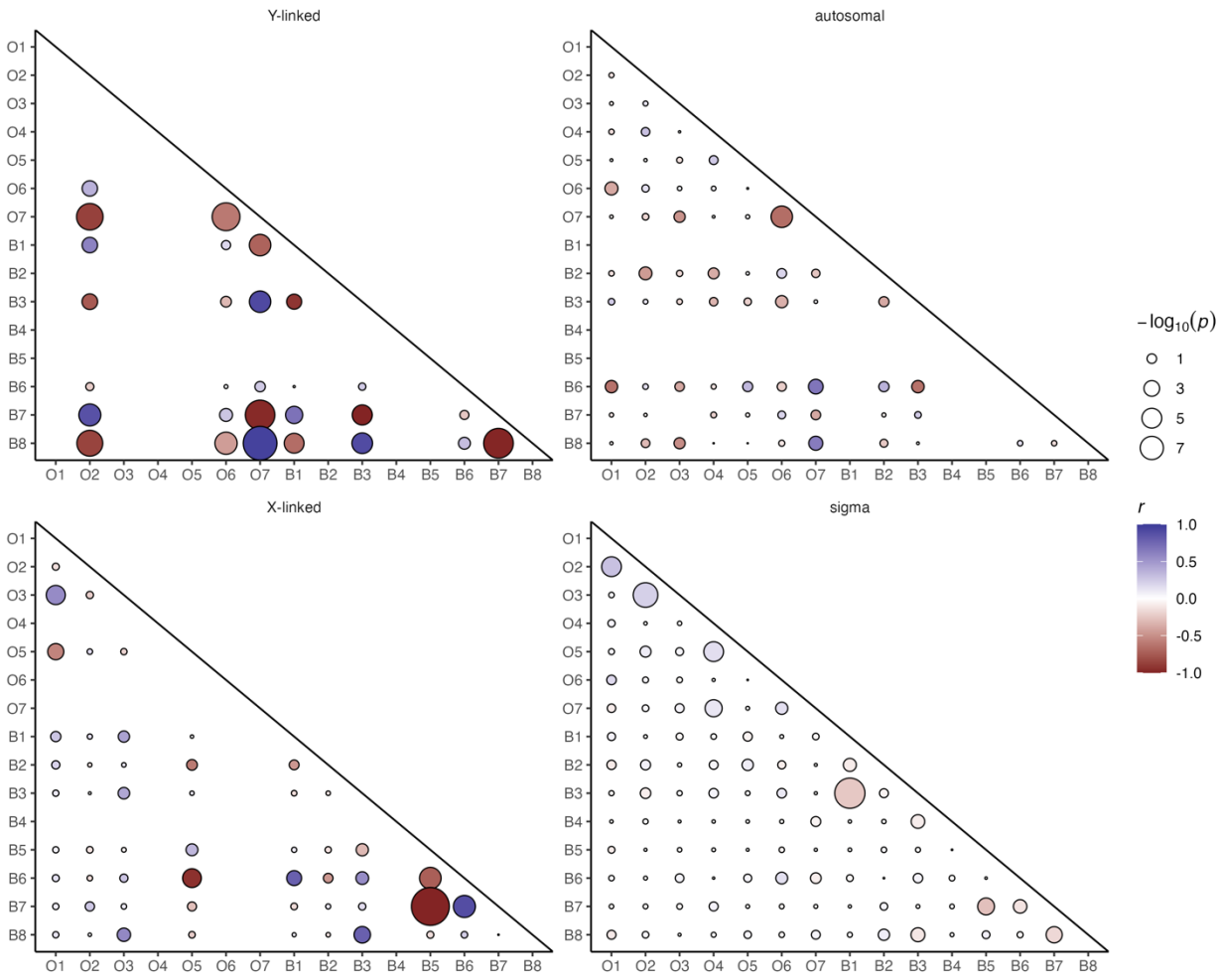

Fig S10: Pairwise correlations of the presence of ornaments, separated in the Y-linked, X-linked and autosomal components, and the environment (sigma). The asymptotic -log10(p-value) of the correlation is shown as the point size, with the color reflecting the estimating correlation coefficient *r*. Correlations are only shown if the variance component was significantly greater than zero for both ornaments.

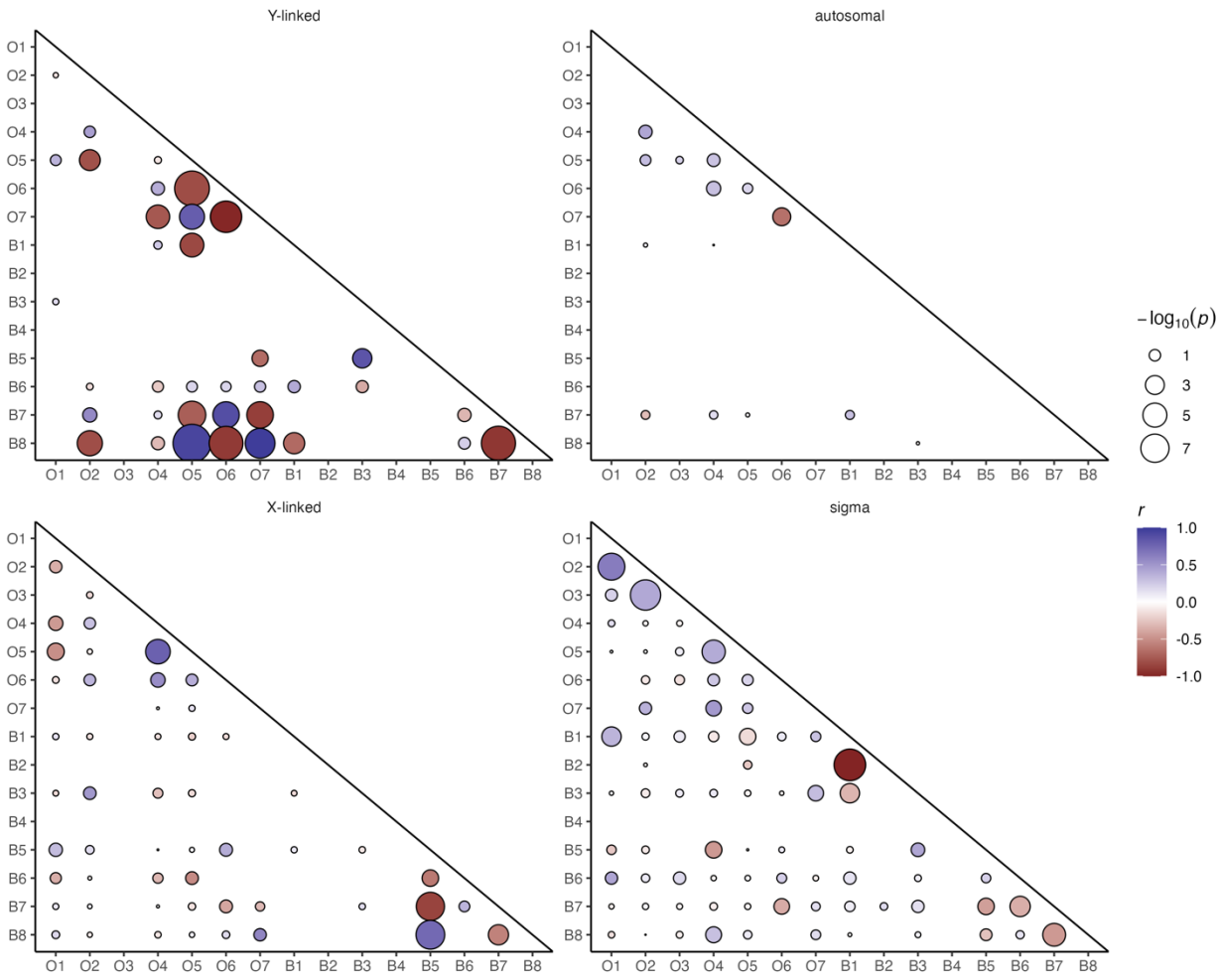

Fig S11: Pairwise correlations of the size of ornaments, separated in the Y-linked, X-linked and autosomal components, and the environment (sigma). The asymptotic -log10(p-value) of the correlation is shown as the point size, with the color reflecting the estimating correlation coefficient *r*. Correlations are only shown if the variance component was significantly greater than zero for both ornaments. Models only included individuals with both ornaments present.

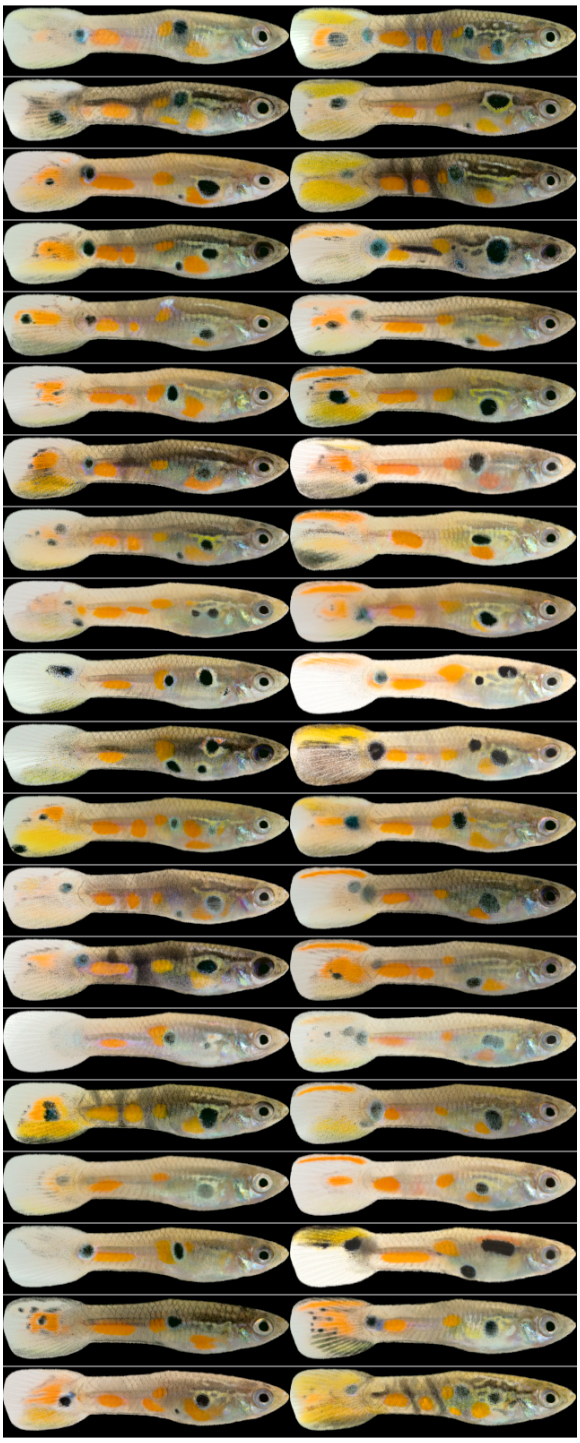

Fig S12: Ornament diversity in the tail fin. Displayed are randomly selected examples of fish with an absent (left) or present (right) ornament O1 (top of the tail fin). Note that the fish with a present ornament O1 have variety of tail ornamentation, possibly indicating spatially overlapping ornaments.

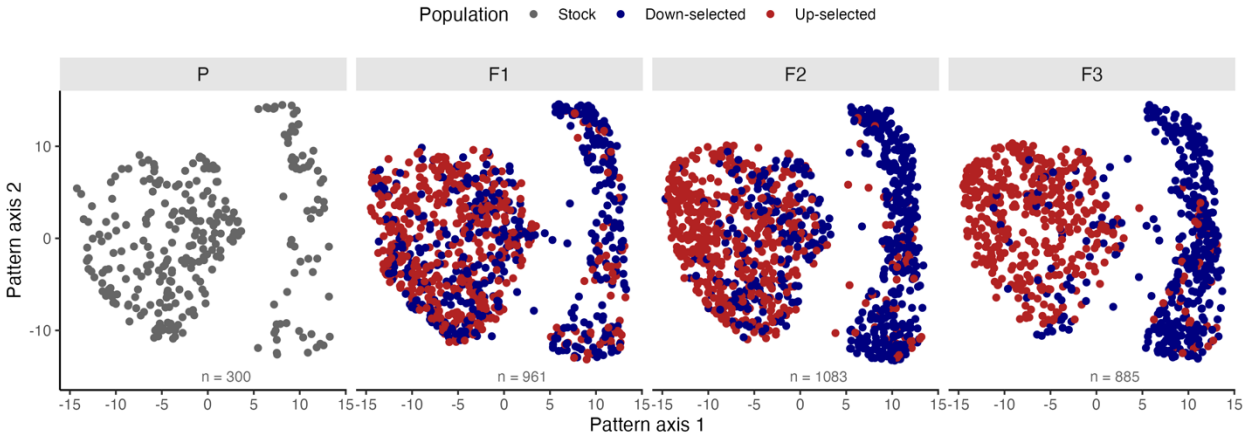

Fig S13: Selection moved populations through orange pattern space. Axes show the UMAP reduced representation of orange pattern space, with points indicating individuals, colored by selection direction, and panel showing the four generations.

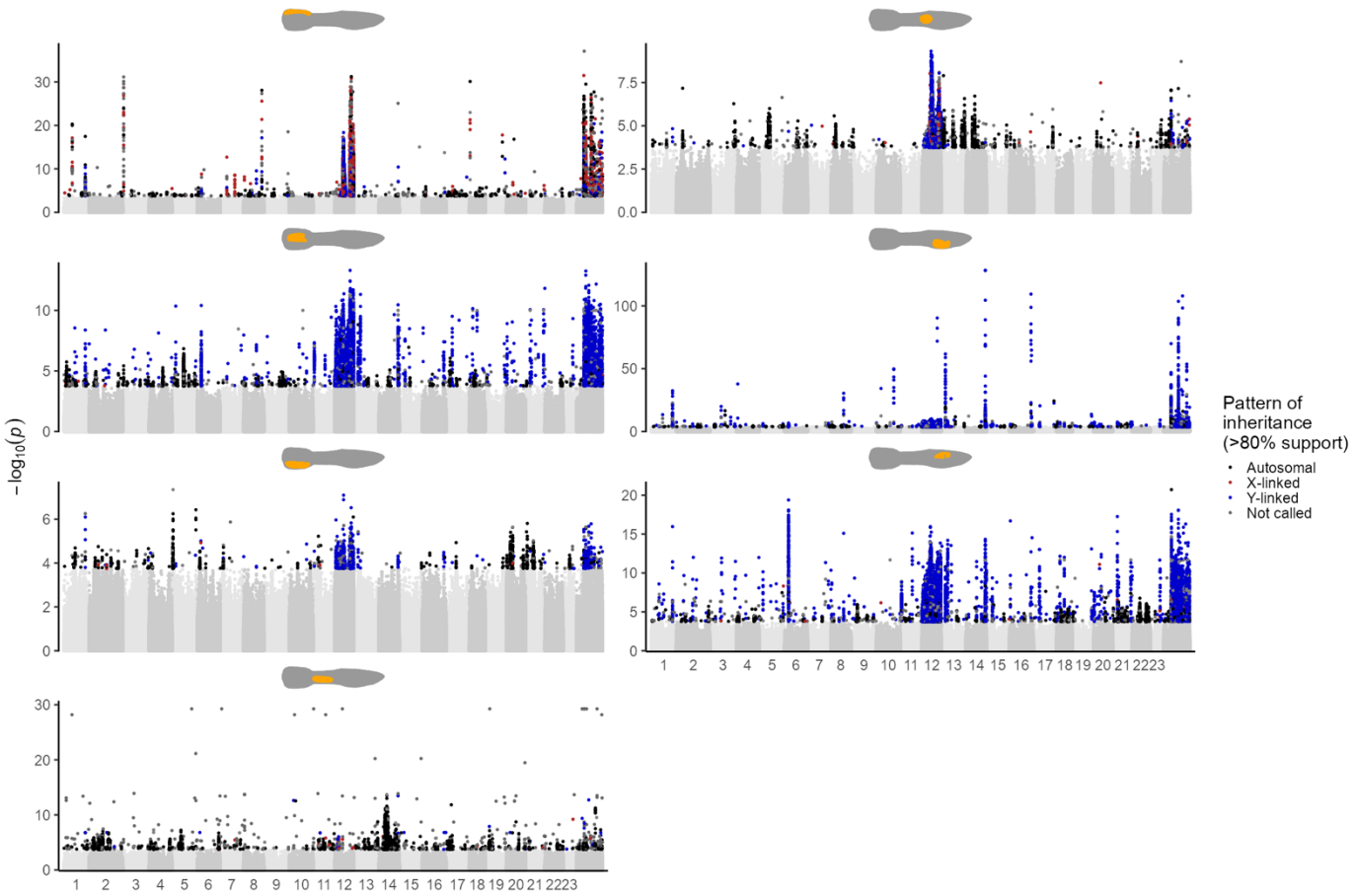

Fig S14: GWAS results for the presence/absence of seven orange ornaments, as in Fig 5. Points represent SNPs and small indels, with their genomic location on the x-axis, and the p-value of the association on the y-axis. Numbers along the x axis denote linkage groups, with unplaced scaffolds plotted on the right-hand side. Significant associations (5% FDR) are colored by their inferred pattern of inheritance, whereas non-significant associations are colored in alternating shades of grey.

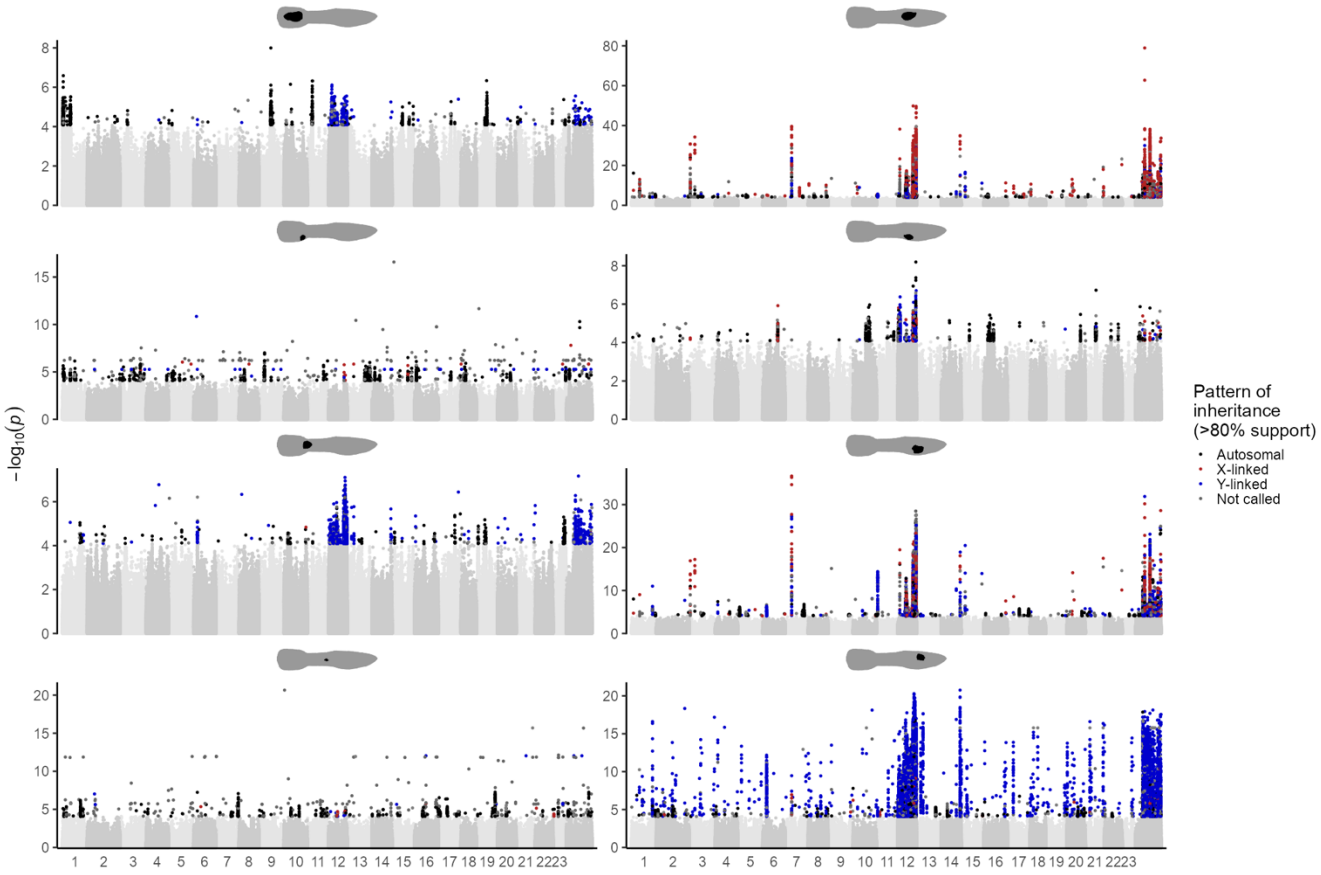

Fig S15: GWAS results for the presence/absence of eight black ornaments, as in Fig 5. Points represent SNPs and small indels, with their genomic location on the x-axis, and the p-value of the association on the y-axis. Numbers along the x axis denote linkage groups, with unplaced scaffolds plotted on the right-hand side. Significant associations (5% FDR) are colored by their inferred pattern of inheritance, whereas non-significant associations are colored in alternating shades of grey.

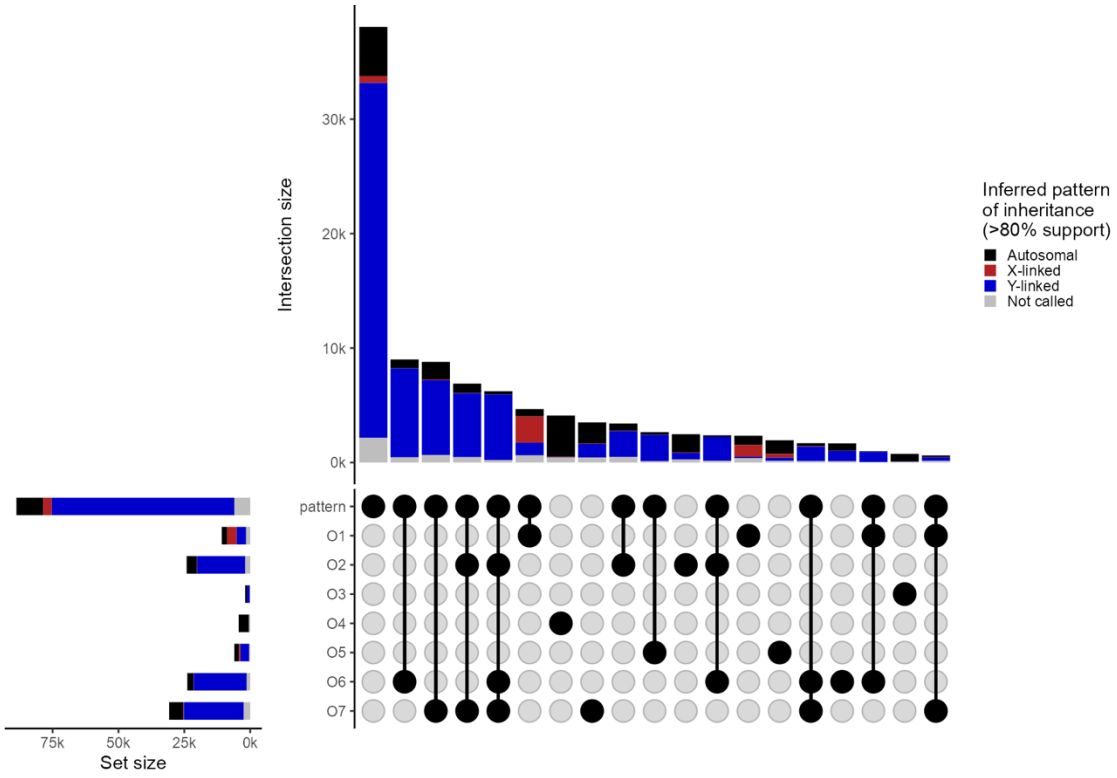

Fig S16: Upset plot showing the unique and overlapping elements in significant variants detected in the GWAS for orange pattern and seven orange ornaments, across the whole genome. Vertical bars represent the count of elements unique or shared between sets, with the connected dot display indicating the specific sets involved in each intersection. Horizontal bars show individual set sizes. Bars are colored proportionally by the inferred inheritance pattern of the variants in that set or intersection. Intersections of fewer than 500 variants not shown.

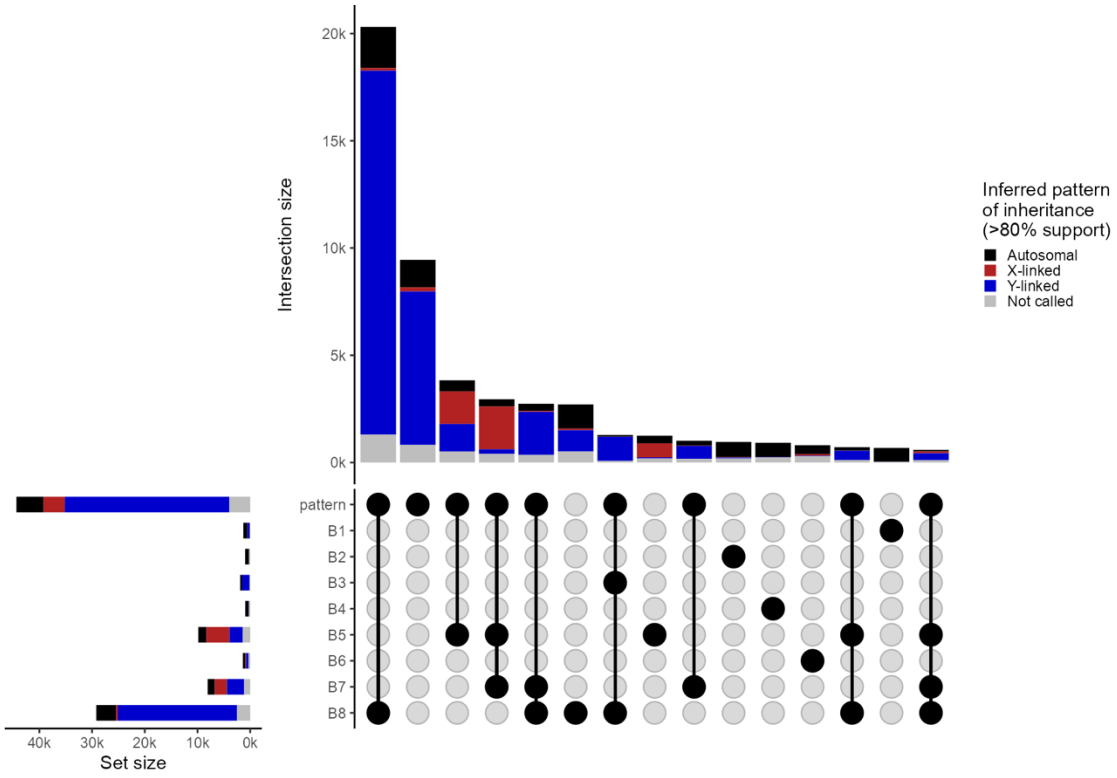

Fig S17: Upset plot showing the unique and overlapping elements in significant variants detected in the GWAS for black pattern and eight black ornaments, across the whole genome. Vertical bars represent the count of elements unique or shared between sets, with the connected dot display indicating the specific sets involved in each intersection. Horizontal bars show individual set sizes. Bars are colored proportionally by the inferred inheritance pattern of the variants in that set or intersection. Intersections of fewer than 500 variants not shown.

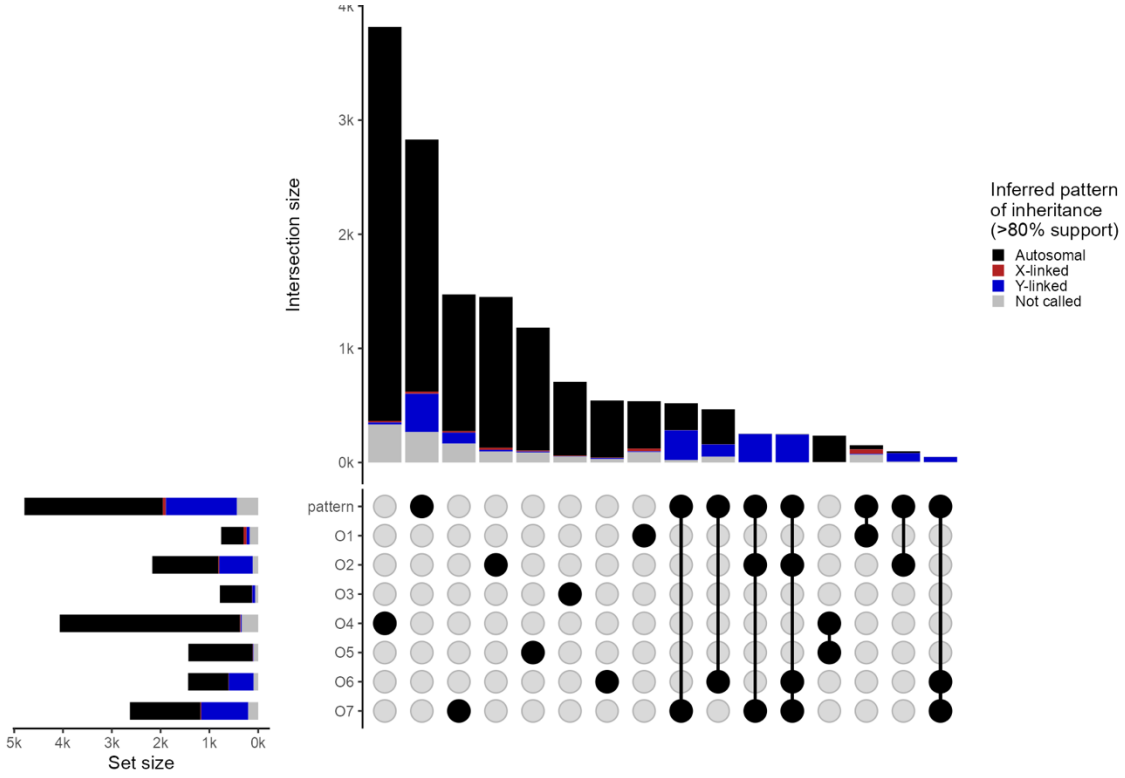

Fig S18: Upset plot showing the unique and overlapping elements in significant variants detected in the GWAS for orange pattern and seven orange ornaments, for variants mapping to the autosomes. Vertical bars represent the count of elements unique or shared between sets, with the connected dot display indicating the specific sets involved in each intersection. Horizontal bars show individual set sizes. Bars are colored proportionally by the inferred inheritance pattern of the variants in that set or intersection. Intersections of fewer than 50 variants not shown.

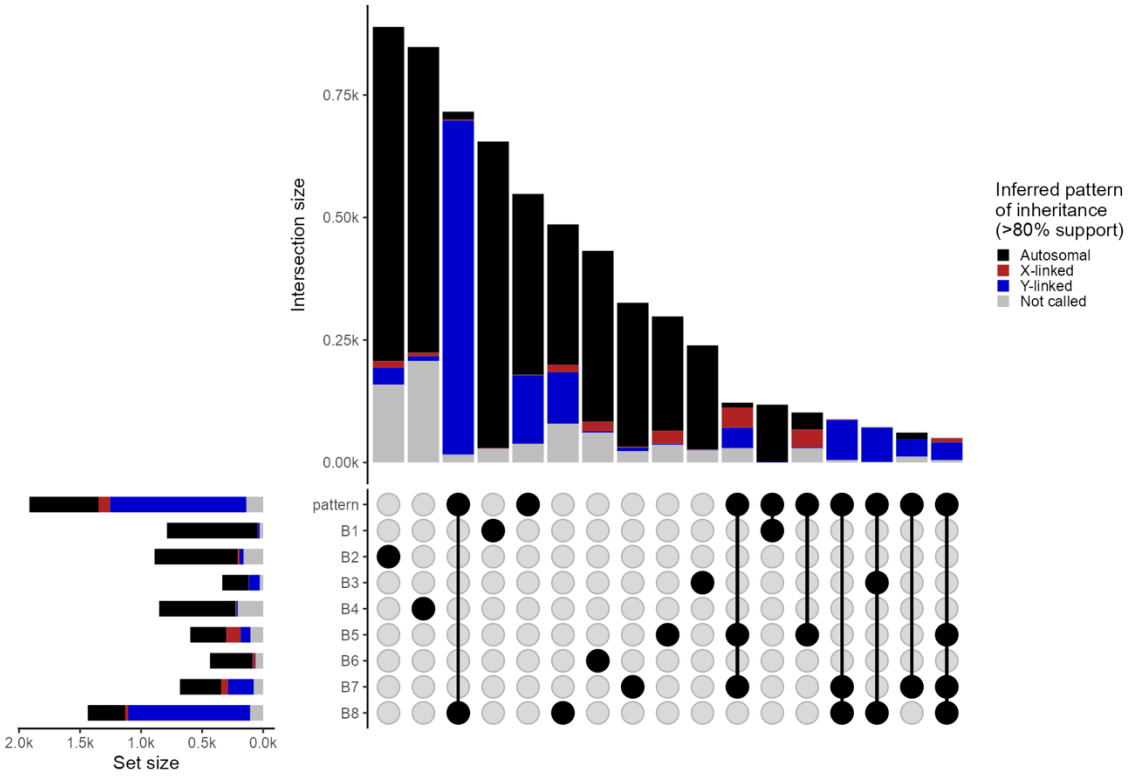

Fig S19: Upset plot showing the unique and overlapping elements in significant variants detected in the GWAS for black pattern and eight black ornaments, for variants mapping to the autosomes. Vertical bars represent the count of elements unique or shared between sets, with the connected dot display indicating the specific sets involved in each intersection. Horizontal bars show individual set sizes. Bars are colored proportionally by the inferred inheritance pattern of the variants in that set or intersection. Intersections of fewer than 50 variants not shown.

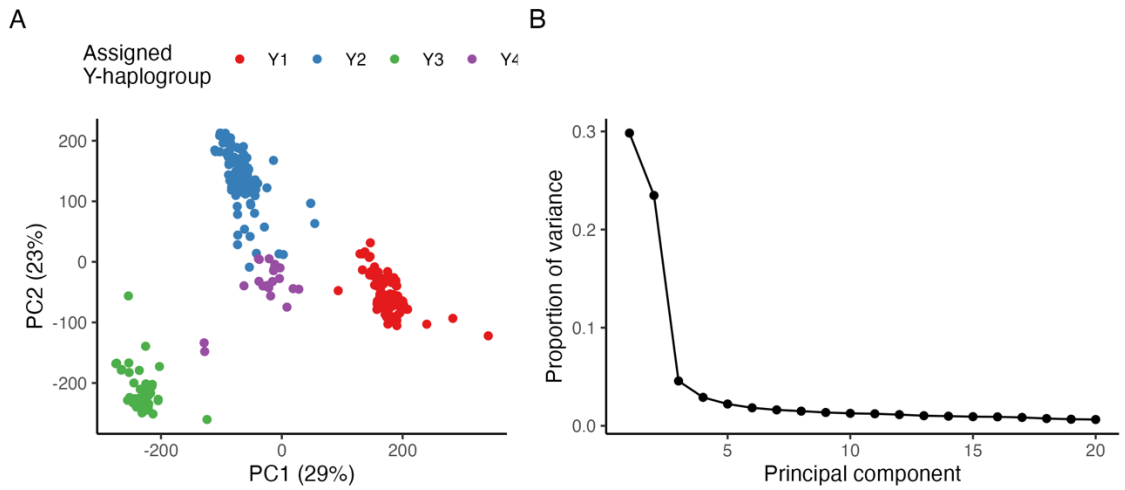

Fig S20: Principal component analysis of variants associated with orange pattern and Y-linked inheritance pattern. A) shows the biplot with labeled inferred Y-haplogroups, while B) shows the scree plot.

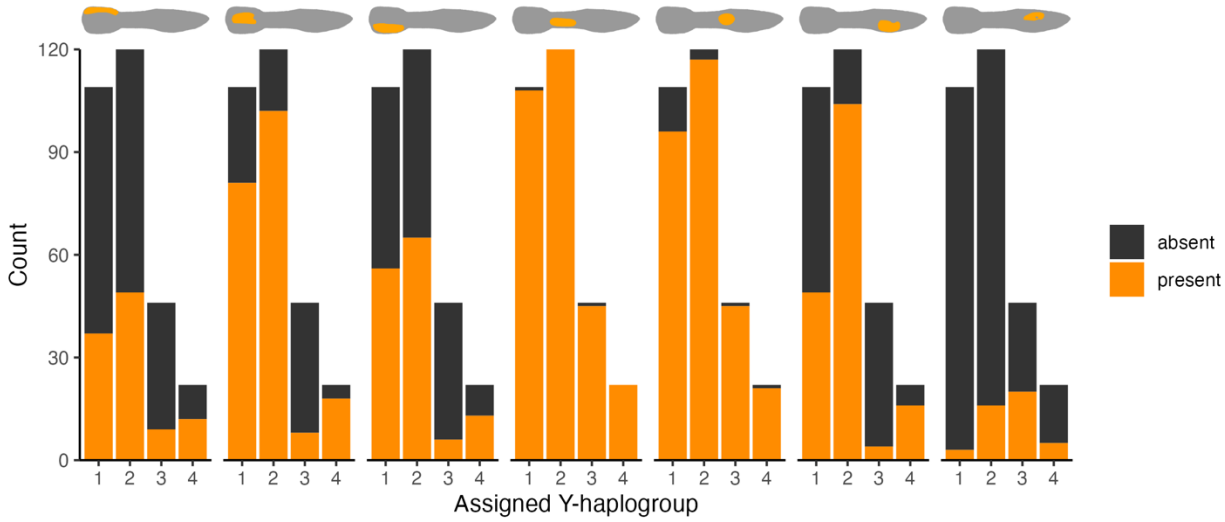

Fig S21: Stacked bar chart showing the relationship between Y-haplogroup and ornament presence.

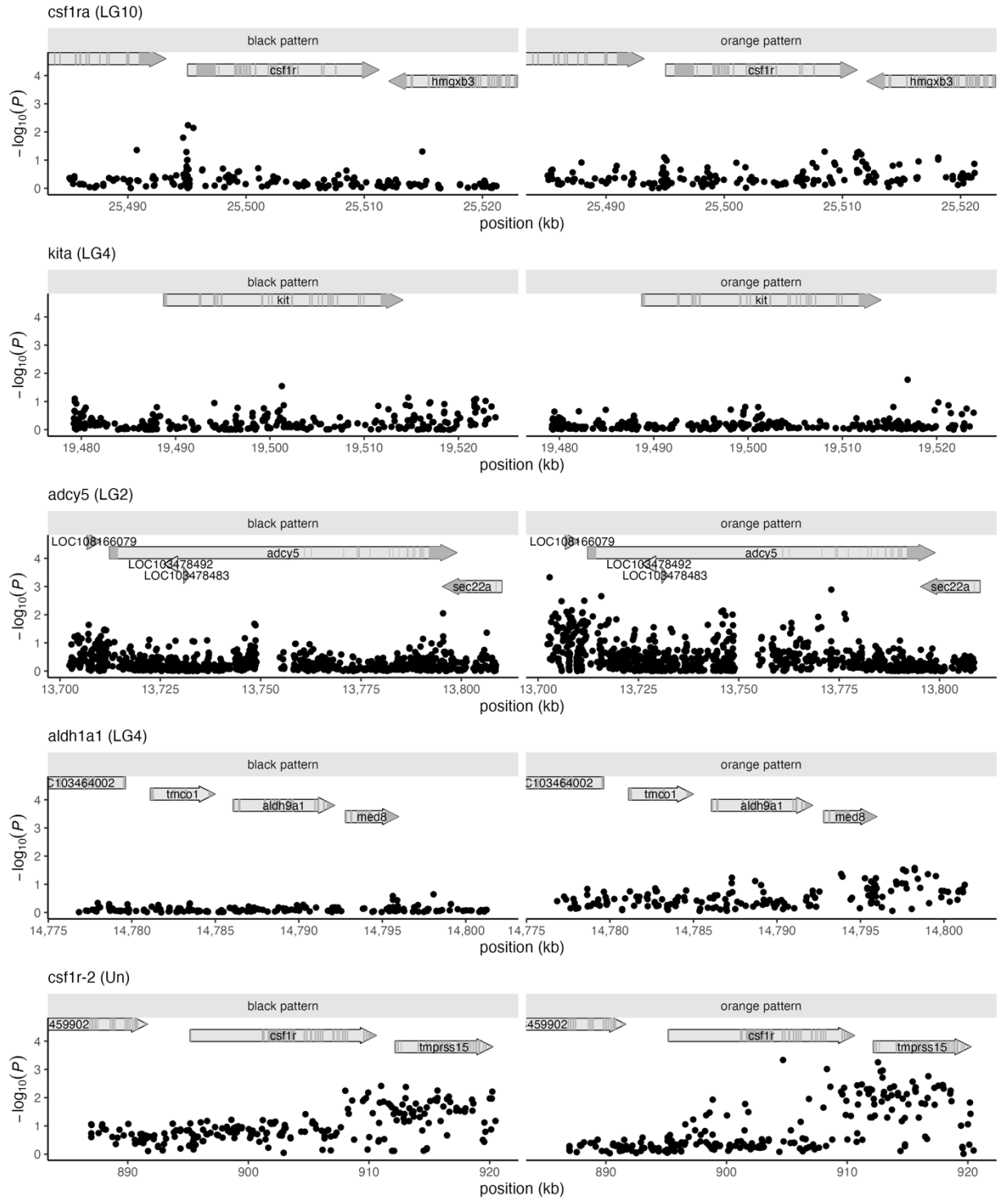

Figure S22: No relationship between black and orange color pattern and genes previously indicated in carotenoid and melanic pigmentation. Panels show GWAS results for black and orange pattern space.

Supplemental tables

Table S1: Architecture of the convolutional neural net used in step 3 of the pipeline.

Layer	Activation	Filters	Output shape	Spatial dropout
Convolution	Relu	32	[400, 144, 32]	0.4
Convolution	Relu	64	[400, 144, 64]	0.4
Max pooling			[200, 72, 64]	
Convolution	Relu	128	[200, 72, 128]	0.4
Deconvolution	Relu	128	[200, 72, 128]	0.4
Upsampling			[400, 144, 128]	
Deconvolution	Relu	64	[400, 144, 64]	0.4
Deconvolution	Linear	4	[400, 144, 4]	